RIGA TECHNICAL UNIVERSITY

Dmitrii Redka

EVALUATION OF DYNAMICS OF NON-SCATTERING STATES IN NANOPHOTONICS

Summary of the Doctoral Thesis

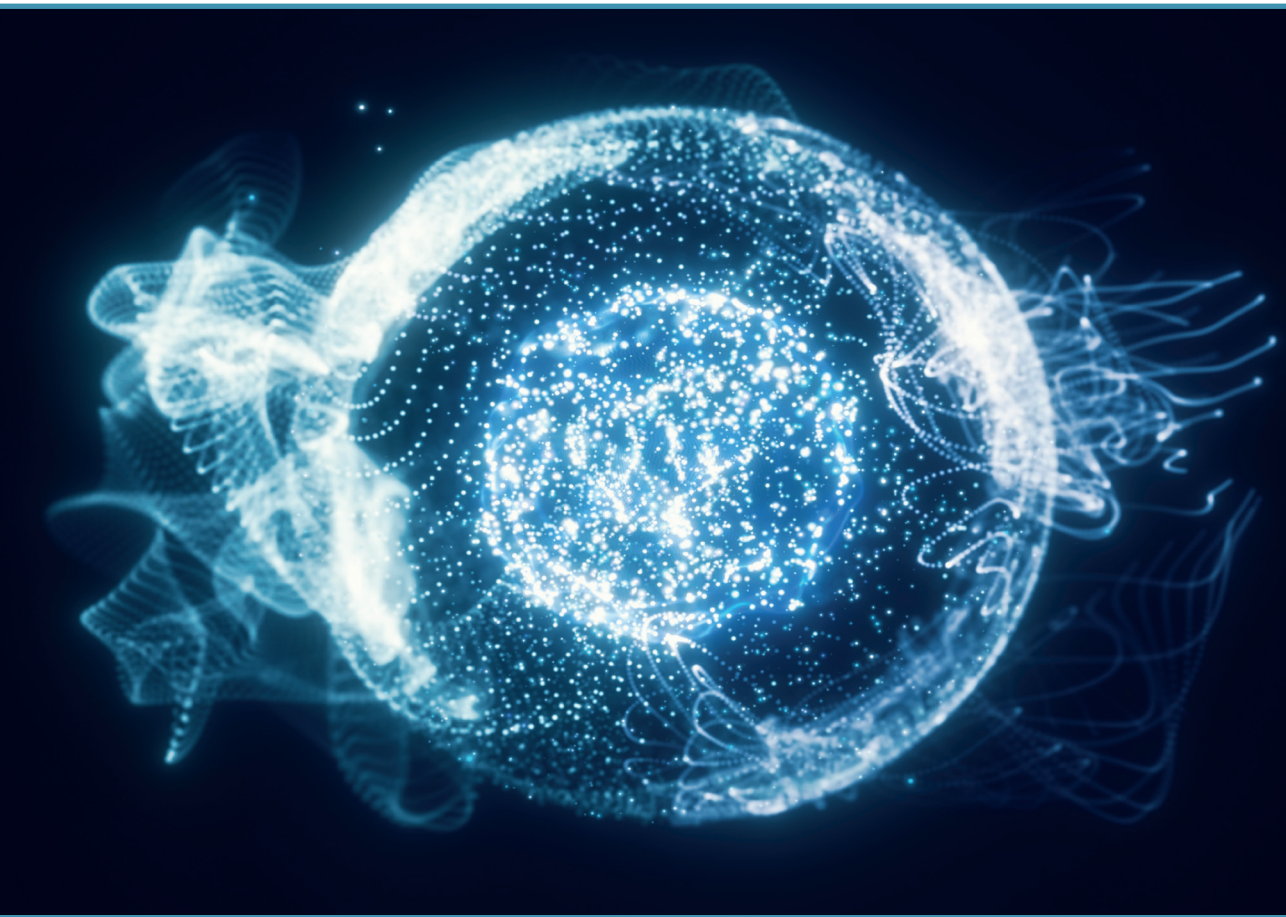

RTU Press
Riga 2024

RIGA TECHNICAL UNIVERSITY
Faculty of Computer Science, Information Technology and Energy
Institute of Photonics, Electronics and Telecommunications

Dmitrii Redka
Doctoral Student of the Study Programme "Telecommunications"

EVALUATION OF DYNAMICS OF NON-SCATTERING STATES IN NANOPHOTONICS

Summary of the Doctoral Thesis

Scientific supervisor
Professor Dr. sc. ing. VJAČESLAVS BOBROVS

RTU Press
Riga 2024

Redka D., Evaluation of Dynamics of Non-Scattering States in Nanophotonics.
Summary of the Doctoral Thesis.
Riga: RTU Press, 2024. 45 p.

Published in accordance with the decision of the Promotion Council
"P- 08" of 24 May 2024,
Minutes No. 32.

This work has been supported by the European Social Fund within Project No. 8.2.2.0/20/I/008, "Strengthening of PhD students and academic personnel of Riga Technical University and BA School of Business and Finance in the strategic fields of specialization" of the Specific Objective 8.2.2 "To Strengthen Academic Staff of Higher Education Institutions in Strategic Specialization Areas" of the Operational Programme "Growth and Employment".

The research was supported by the Doctoral Grant Programme of Riga Technical University.

https://doi.org/10.7250/9789934371004

ISBN 978-9934-37-100-4 (pdf)

DOCTORAL THESIS PROPOSED TO RIGA TECHNICAL UNIVERSITY FOR PROMOTION TO THE SCIENTIFIC DEGREE OF DOCTOR OF SCIENCE

To be granted the scientific degree of Doctor of Science (Ph. D.), the present Doctoral Thesis has been submitted for defense at the open meeting of the RTU Promotion Council on 30 August 2024 at the Faculty of Computer Science, Information Technology and Energy of Riga Technical University, 12 Azenes Str., Room 201.

OFFICIAL REVIEWERS

Researcher, Ph. D. Inga Brice
University of Latvia, Latvia

Professor, Ph. D, Lei Gao
Soochow University, China

Professor, Dr. sc. ing. Jurģis Poriņš
Riga Technical University

DECLARATION OF ACADEMIC INTEGRITY

I hereby declare that the Doctoral Thesis submitted for review to Riga Technical University for promotion to the scientific degree of Doctor of Science (Ph. D.) is my own. I confirm that this Doctoral Thesis has not been submitted to any other university for promotion to a scientific degree.

Dmitrii Redka ……. (signature)

Date: ……

The Doctoral Thesis has been prepared as a thematically united collection of scientific publications. It comprises 11 scientific articles and publications in conference proceedings indexed in SCOPUS, WoS, and IEEE databases. Publications are written in English and are published in SCOPUS, WoS, and IEEE databases; their total volume/number of pages is 105 pages.

LIST OF ABBREVIATIONS

BICs – Bound States in the Continuum

CW – Continuous Wave

EDA – Electric Dipole Anapole

HA – Hybrid Anapoles

HM – Hyperbolic Modes

LOCP – Lab-On-a-Chip Platforms

LTIE – Low-Temperature Ion Exchange

MOCT – Magnetic Octupole

MSAD – Mean-Squared Angular Displacements

OAM – Orbital Angular Momentum

QNM – Quasi-Normal Modes

SIT – Self-Induced Transparency

SAM – Spin Angular Momentum

SMR FBARs – Solid Mounted Film Bulk Acoustic Resonators

SOC – Spin-Orbit Couplings

SPP – Surface Plasmon-Polariton

WGM – Whispering Gallery Mode

CONTENTS

1. GENERAL OVERVIEW OF THE THESIS

1.1. Introduction

In the last decade, the interest in the optical properties of structures of high-index semiconductor nanoparticles with low losses (for example, Si, TiO_2) increased incrementally [1]. Their response in a continuous irradiation mode was studied in detail, and many new optical effects were obtained, arising primarily due to the ability to excite both electrical and magnetic multipole moments in such particles and the almost complete absence of absorption [2], [3]. Based on the detected phenomena, several ultra-thin optical systems (about a few tens of nanometers thick) have been developed [4], [5], [6]. These systems have functionality that is unattainable for the conventional ones. Despite the large number of groups in the world carrying out these studies, the field still is far from exhaustion, being regularly replenished with new discoveries.

It seems most interesting to consider the temporal dynamics of states that in the stationary mode are non-scattering (dark modes) and, accordingly, the metasurfaces of such particles are almost completely transparent. In this regard, nanoparticles and metasurfaces in the anapole and hybrid-anapole states (the recently discovered state protected in a stationary regime from both the environment and the substrate, the femtosecond response of which, in turn, strongly depends on the environment and substrate [7]) will be investigated theoretically and experimentally. These states, similar in stationary mode, have completely different mode compositions and will allow realizing different time dynamics and effects. The combination of the completely different properties in continuous and pulse regimes will provide an opportunity to subsequently develop new optical elements with dual functionality (for example, new ultra-thin repetition rate multipliers, light filters, modulators, polarizers, etc.), which presently do not exist.

The planned Thesis lies in a new and extremely rapidly developing field of nanophotonics [8–10]. For example, according to the Scopus database, more than 1,500 articles are published annually in this area. The applications of dielectric nanophotonics are very diverse; for example, waveguides [11], [12], modulators [13], directional radiation sources and nanoantennas [14], detectors [15], masking and invisibility devices [16], phase metasurfaces [17], [18], etc. The development of dielectric nanophotonics has already made it possible to create various metasurfaces, materials, and meta-devices that realize the control of optical beams with almost no loss [19].

However, there is now a need for new, ultra-thin photonic elements capable of effectively controlling ultrashort laser pulses, which the aforementioned nanophotonic devices, with few exceptions, do not allow [20].

The PhD Thesis is complex and includes a full cycle of work, starting with a theoretical (analytical and numerical) study of the tasks, carried out in close cooperation with the experimental testing, which will make it possible to verify the correctness of the theory and, if necessary, make adjustments to it, and ending with the testing of prototypes that most fully demonstrate new phenomena, this project is devoted to. Specifically, the Thesis is investigating

both theoretically and experimentally new effects due to the action of ultrashort laser pulses on high-index semiconductor nanoparticles (e.g., Si, Ge) with low absorption in the visible range. Currently, this area remains poorly explored. The study of transient dynamics in interaction with the pulses of nanoparticles in states that are non-scattering relative to continuous radiation, characterized by non-trivial mode structure in the near field, is of special interest. In particular, the project will focus on the study of the temporal dynamics of the anapole and hybrid-anapole states, as well as the interaction of metasurfaces of such nanoparticles with femtosecond pulses. Note that it is, for the first time, found that at the steady-state, the mentioned new hybrid anapole may correspond to the realization at the same frequency of the anapole states simultaneously for all contributing multipoles. Therefore, the irradiated particles occur in a completely non-scattering state (the usual anapole state makes it possible to extinguish only the radiation from a single, usually electric-dipolar, mode).

Remarkably, a hybrid anapole state is accompanied by a strong concentration of the electromagnetic field in the near field zone and the excitation of a large set of resonant and non-resonant eigenmodes with different Q-factors. At the action of a short (femtosecond) laser pulse, it may result in a strong and non-trivial modulation of its envelope. In the case of the irradiation of an array of such nanoparticles and/or the corresponding metasurfaces, the modulation will depend on the metasurface's symmetry as well as on the geometrical and optical properties of the substrate. Note that in the CW irradiation the optical response in the hybrid-anapole state does not depend on the environment and the substrate. Because of that, the metasurfaces made of such nanoparticles, while remaining completely transparent to a CW (though controlling its phase!), should strongly modulate femtosecond pulses. These properties will be used in the project to realize various dual-performance optical systems and devices whose response to the action of femtosecond and long laser pulses will be qualitatively different.

The focus is on the study of new optical effects in the challenging subfield of ultrafast subwavelength optics. However, the specific subfield, namely transient optics of the non-scattering regimes, practically has not been developed yet and represents a vast field of activity. The Thesis is aimed at fundamental research in a new area and the implementation of fundamental models of new devices based on the results obtained. Within the Thesis framework, models have been developed, and prototypes of new ultra-thin planar photonic elements such as ultra-thin repetition rate multipliers, light filters, beam modulators, etc., have been implemented. These elements are designed for femtosecond optics and have dual-use applications for both short pulses and continuous irradiation.

1.2. The aim and theses of the dissertation

Summarizing the above-mentioned facts about the directions of development of semiconductor nanostructures and their applications in photonic devices and optical communication systems, the following aim of the Doctoral Thesis is proposed: Study and explore new optical effects arising from the interaction of semiconductor nanoparticles with metasurfaces when exposed to femtosecond laser pulses. Develop new models of

nanostructured elements and evaluate their potential applications in modern telecommunication systems and photonics.

To achieve the aim set, the following theses were put forward:

1. The current theory of hybrid anapole conditions demonstrates that effective spatiotemporal control of transients mediated by the underlying substrate can be achieved while maintaining scattering at negligible levels in the stationary regime.

2. High-k volumetric modes can provide additional channels for the particles' interaction with substrates, thereby significantly enhancing the capabilities of optomechanical manipulation schemes. For semi-infinite (or rather thick) metamaterial slabs, the hyperbolic modes, even though dominant in scattering, do not contribute to optical binding due to the almost absent feedback. Hyperbolic modes excited by one particle do not interact with the second one. In contrast, thin metamaterial slabs provide multiple reflections from boundaries, forming a set of strongly localized hot spots with significant intensity gradients that govern nanoparticles' motion at the nanoscale.

3. The dynamics of the time-dependent Purcell effect in a solution of phosphorescent molecules interfacing resonant nanoantenna can be utilized for contactless all-optical temperature and diffusion measurements. The dynamics of the long-life-time phosphorescent molecule’s decay is shown to be strongly dependent on the Brownian motion next to a resonator. This special interaction is described with the temperature and diffusion coefficient of the surrounding liquid. Subsequently, far-field radiation emitted from diffusing molecules is analyzed via the inverse Laplace transform and exploited to recover the local properties of a fluid environment.

4. A resonant magnetic octupole (MOCT) response can be obtained by dividing a solid rectangular silicon block into a quadrumer structure with the introduction of narrow gaps between four nanocubes. The spectral position of the MOCT resonance is controlled and tuned by varying the distance between the nanocubes.

5. Bound states in the continuum (BICs) enable unique features in tailoring light-matter interaction on the nanoscale. These radiationless localized states drive theoretically infinite quality factors and lifetimes for modern nanophotonics, making room for a variety of emerging applications.

1.3. The key tasks of the Doctoral Thesis

To achieve the set goal of the dissertation and to prove the proposed theses, it is necessary to perform the following key tasks:

1. Theoretically predict and experimentally confirm the existence of hybrid anapoles, previously unnoticed non-scattering regimes requiring the simultaneous destructive interference of electric and magnetic cartesian multipoles with their toroidal counterparts. Establish a more in-depth view of the hybrid anapole by comparing it to its simpler counterpart, the electric dipole anapole, and validate an alternative description of conventional anapole states based on the Fano response's separation into a resonant and a non-resonant contribution.

2. Perform a theoretical study of the dynamic time-dependent Purcell effect in a solution of phosphorescent molecules interfacing with a resonant nanoantenna.

3. Study the propagation of ultrashort pulses in the resonant multilayered medium with initial population difference randomly varying along the propagation direction. Consider three potential disorder models and reveal their potential applications for flexible control over the optical response of the medium.

4. Analyze conditions for maximal conversion of spin angular momentum of the incident light to orbital angular momentum of the scattered light via the specially designed transversely scattering silicon nanocube.

1.4. Research methods

To perform the tasks outlined in the Doctoral Thesis and to analyze the problems, mathematical calculations, numerical simulations, and experimental measurements have been used. Numerical simulations were implemented in Matlab, Origin, Comsol Multiphysics, CST MICROWAVE STUDIO, and Ansoft Academic Research HF.

Scientific experiments described in the Doctoral Thesis and their results were carried out at the Nanophotonics Research Laboratory (NANO-Photon Lab) at the Institute of Photonics, Electronics and Telecommunications (IPET) of Riga Technical University (RTU), the St. Petersburg Electrotechnical University (ETU "LETI", Russia), Information Technologies, Mechanics and Optics University (ITMO, Russia), and the University of Graz (Austria).

1.5. Scientific novelty and main results

Novel achievements of the Doctoral Thesis are as follows:

1. The author theoretically predicted and experimentally confirmed the existence of hybrid anapoles, previously unnoticed non-scattering regimes requiring the simultaneous destructive interference of electric and magnetic cartesian multipoles with their toroidal counterparts. In the transient regime, obtained results have allowed to design at will the breakdown of the hybrid anapole conditions to obtain ultrafast modulation of the scattered power. Therefore, combining findings with up-to-date modulation techniques holds great promise for future applications in the emerging field of ultrafast dynamic nanophotonics.

2. For the first time, higher-order (quadrupolar) toroidal moments are shown to contribute to essential features of the scattering response of an isolated high-index nanoparticle. The author validated results by fabricating a series of individual silicon nanocylinders supporting the HA and confirmed its existence experimentally through dark-field spectroscopy measurements.

3. The author investigated the propagation of ultrashort pulses in a resonant multilayered medium with randomly varying initial population differences along the propagation direction. As a result, three potential disorder models were considered, revealing two transitions and three distinct regimes as the disorder increased. The transitions were from the self-induced transparency (SIT) regime to the localization regime and then to the amplification regime. The amplification regime only appeared when negative population differences were possible, and

the disorder was sufficiently large. These effects provide opportunities for flexible control over the optical response of the medium, enabling adjustments in the reflection-to-transmission ratio and pulse propagation speed through the disorder parameter.

4. The author developed a novel concept for contactless temperature and diffusion measurements utilizing the Purcell effect in phosphorescent molecules near a nanoantenna. By analyzing the emitted radiation, we can extract the local properties of the surrounding liquid, enabling efficient and high-resolution measurements across a wide temperature range. This method has potential applications in lab-on-a-chip systems and microfluidics.

5. The author demonstrated novel superscattering regimes by utilizing subwavelength, nonspherical resonators and exploiting the strong coupling of two resonances. The findings show superscattering originating from an electric super dipole moment, surpassing the currently established limit by almost two times. By disrupting the quasi-BIC condition in resonators without spherical symmetry through parameter adjustments, power exchange between scattering channels enables the manipulation of Q-factors and multipolar contents while maintaining a high scattering cross-section. The super multipole resonances exhibit enhanced resistance to Ohmic losses compared to conventional counterparts. These findings have implications in biosensing, energy harvesting, on-chip circuitry and optical manipulation.

1.6. The practical value of the Doctoral Thesis

1. A new cost-effective material suitable for use in label-free sensors with active WGM resonators has been obtained. The experiment showed that glass samples subjected to low-temperature ion exchange (LTIE) showed distinct absorption characteristics, particularly the absence of characteristic absorption peaks, which was attributed to the formation of Ag2...5 molecular clusters of silver. According to the simulation results, the difference between the resonant wavelengths for media with different refractive indexes was 0.26 nm. This allows the material to be used for microsphere sensors without a direct physical connection. The results obtained show the potential of soda silicate glass with molecular silver clusters as a material for WGM sensors.

2. Resonant MOCT excitation has been confirmed to induce controlled magnetic hotspots and resonant absorption in a nanostructure. Utilizing quadrumers as building blocks for metasurfaces holds the promise of achieving even greater magnetic field enhancement thanks to the potential excitation of trapped modes. Moreover, after being scaled to the microwave region, the considered structure could be very promising for magnetic resonance imaging applications. Additionally, the resonant magnetic octupole response can be extensively utilized for spectroscopy, sensing, detecting small quantum objects, and various other potential applications.

3. The Thesis demonstrated the results of theoretical research work focused on studying technologically competitive solutions of phononic structures' performance for the purposes of FBAR devices. Computational results for square, triangular, and honeycomb arrangements demonstrating the achievable bandgap responses have been presented. It was found that the

honeycomb arrangement is the most advantageous in terms of bandgap performance, which should allow the FBAR structures to operate within a broad frequency range.

The results obtained in the dissertation were used in the following projects:

1. Novel non-Hermitian singularities in all-dielectric nanostructures (NEO-NATE) (01.01.2023–31.12.2025).
2. Strengthening of PhD students and academic personnel of Riga Technical University and BA School of Business and Finance in the strategic fields of specialization (01.08.2021–30.11.2023).
3. Deutsche Forschungsgemeinschaft (DFG, German Research Foundation) within the Cluster of Excellence PhoenixD (EXC 2122, Project ID 390833453).

1.7. Structure of the Thesis

The dissertation is prepared as a thematically unified set of publications on the development and evaluation of quantum effects in nanostructures that can be used in future more efficient hybrid optical communication systems and their elements.

Chapter 1 describes the topicality of the research, evaluates the aim and theses, describes the main tasks, research methodology, the structure of the work and the main results.

Chapter 2 describes the results of theoretical and numerical studies, as well as modeling new optical effects in nanostructured environments. The main stages are:

1. Multipole analysis of hybrid anapoles (contribution from PAPER 1).
2. Study of nanoparticle dynamics (contribution from PAPERS 2 and 9).
3. Study of ultrashort pulse propagation in nanostructured environments (contribution from PAPER 8).
4. Modeling optical effects in nanostructured environments (contribution from PAPERS 3, 4, 6, 9, 10).

Chapter 3 focuses on experimental research on optical sensors and the study of new nanomaterials (contribution from PAPERS 7 and 11).

In Conclusions, both theoretical and experimental results are discussed, and answers to the established questions are given.

1.8 Publications and approbation of the Thesis

The results of the Doctoral Thesis are presented in 11 scientific articles and conference proceedings indexed in SCOPUS, WoS, and IEEE databases. The author has 39 publications overall.

PAPER 1. Canós Valero, A., Gurvitz, E. A., Benimetskiy, F. A., Pidgayko, D. A., Samusev, A., Evlyukhin, A. B., Bobrovs, V., Redka, D., Tribelsky, M. I., Rahmani, M., Kamali, K. Z., Pavlov, A. A., Miroshnichenko, A. E., Shalin, A. S. “Theory, Observation, and Ultrafast Response of the Hybrid Anapole Regime in Light Scattering”, (2021) Laser and Photonics Reviews, 15 (10), art. no. 2100114, DOI: 10.1002/lpor.202100114

PAPER 2. Canós Valero, A., Kislov, D., Gurvitz, E. A., Shamkhi, H. K., Pavlov, A. A., Redka, D., Yankin, S., Zemánek, P., Shalin, A.S. “Nanovortex-Driven All-Dielectric Optical Diffusion Boosting and Sorting Concept for Lab-on-a-Chip Platforms”, (2020) Advanced Science, 7 (11), art. no. 1903049, DOI: 10.1002/advs.201903049

PAPER 3. Novitsky, D. V., Shalin, A. S., Redka, D., Bobrovs, V., Novitsky, A. V. “Quasibound states in the continuum induced by PT symmetry breaking”, (2021) Physical Review B, 104 (8), art. no. 085126, DOI: 10.1103/PhysRevB.104.085126

PAPER 4. Terekhov, P. D., Evlyukhin, A. B., Redka, D., Volkov, V. S., Shalin, A. S., Karabchevsky, A. “Magnetic Octupole Response of Dielectric Quadrumers”, (2020) Laser and Photonics Reviews, 14 (4), art. no. 1900331, DOI: 10.1002/lpor.201900331

PAPER 5. Novitsky, D. V., Lyakhov, D., Michels, D., Redka, D., Pavlov, A. A., Shalin, A. S. “Controlling wave fronts with tunable disordered non-Hermitian multilayers”, (2021) Scientific Reports, 11 (1), art. no. 4790, DOI: 10.1038/s41598-021-84271-0

PAPER 6. Kostina, N. A., Kislov, D. A., Ivinskaya, A. N., Proskurin, A., Redka, D. N., Novitsky, A., Ginzburg, P., Shalin, A. S. “Nanoscale Tunable Optical Binding Mediated by Hyperbolic Metamaterials”, (2020) ACS Photonics, 7 (2), pp. 425–433, DOI: 10.1021/acsphotonics.9b01378

PAPER 7. Oseev, A., Mukhin, N. V., Lucklum, R., Zubtsov, M., Schmidt, M.-P., Redka, D., Kozyrev, A., Hirsch, S. “Towards macroporous phononic crystal-based structures for FBAR applications. Theoretical investigation of technologically competitive solutions”, (2018) Microsystem Technologies, 24 (5), pp. 2389–2399, DOI: 10.1007/s00542-017-3616-1

PAPER 8. Novitsky, D. V., Redka, D., Shalin, A. S. “Different Regimes of Ultrashort Pulse Propagation in Disordered Layered Media with Resonant Loss and Gain”, (2019) Annalen der Physik, 531 (9), art. no. 1900080, DOI: 10.1002/andp.201900080,

PAPER 9. Kislov, D., Novitsky, D., Kadochkin, A., Redka, D., Shalin, A. S., Ginzburg, P. “Diffusion-inspired time-varying phosphorescent decay in a nanostructured environment”, (2020) Physical Review B, 101 (3), art. no. 035420, DOI: 10.1103/PhysRevB.101.035420

PAPER 10. Canós Valero, A., Shamkhi, H. K., Kupriianov, A. S., Weiss, T., Pavlov, A. A., Redka, D., Bobrovs, V., Kivshar, Y., Shalin, A. S. “Superscattering emerging from the physics of bound states in the continuum”, (2023) Nature Communications, 14 (1), art. no. 4689, DOI: 10.1038/s41467-023-40382-y

PAPER 11. Mikharev, E., Lunev, A., Sidorov, A., Redka, D. “Modeling and Characterization of Microspheres with Silver Molecular Clusters for Sensor Applications”. (2023) Eng. Proc., 58, 95. DOI: 10.3390/ ecsa-10-16196

2. INVESTIGATING AND MODELING NEW OPTICAL EFFECTS IN NANOSTRUCTURED ENVIRONMENTS

2.1. Observation and multipole analysis of hybrid anapoles

All-dielectric nanophotonics, a key area in nano-optics research [21], [22], offers a solution to the ohmic losses found in plasmonic structures by utilizing low-loss semiconductor or dielectric materials such as Si, TiO2, Ge, and GaAs [23], [24]. These materials enable the manipulation of light's electrical and magnetic components at the nanoscale, resulting in applications in low-loss waveguides [25], [26], directional sources [27], [28], harmonic generation [29], light harvesting, and anti-reflective coatings [30]–[32]. Advances also include all-dielectric metasurfaces [33]–[36], beam deflectors [37], and subwavelength fluid mixing [19]. Critical to controlling light at the nanoscale is accurately describing electromagnetic scattering. This is achieved through electromagnetic multipole expansion methods [38]–[42] and the charge-current Cartesian decomposition [38]–[40], which enables the identification of the toroidal moment family within optical properties [41]–[44].

The transient behavior of electric dipole anapole (EDA) remains largely unexplored, despite its potential for novel applications in ultrafast dynamic resonant phenomena. Most studies have focused solely on the stationary response and the electric dipole term [47]–[50]. However, the existence of magnetic anapoles could lead to enhanced radiation suppression and unprecedented electromagnetic energy confinement, opening new possibilities for light-matter interactions, as well as the creation of so-called hybrid anapoles (HA). Recent theoretical advancements [40]–[46] have enabled the investigation of higher-order electric and magnetic anapoles in scatterers with arbitrary shapes, paving the way for further exploration in the field.

This chapter focuses on the design of hybrid anapole configurations and experimentally demonstrates their existence. We demonstrate the emergence of anapoles, which result from multipoles of alternating electric and magnetic nature, interconnected in scatterers with disrupted spherical symmetry. This metasurface combines full transparency in the stationary regime with a highly tunable spatiotemporal response in the transient regime.

The design methodology is based on the following: We note that the spectral positions of the full (basic together with toroidal contributions), electric dipole, and magnetic quadrupole anapoles are mainly dependent on the cylinder's radius. In contrast, the wavelengths of the full magnetic dipole and electric quadrupole anapoles change as functions of both the cylinder height and radius. Thus, carefully tuning these two geometrical degrees of freedom makes it possible to place the anapoles of all the leading terms ultimately close to each other (Fig. 1 b), providing a strong scattering minimum (Fig. 1 b). The measured scattering spectra exhibit a pronounced dip (Fig. 1 c) that shifts with the nanocylinder diameter, which is in agreement with theoretical predictions. The most pronounced hybrid anapole mode occurs at a diameter of 251 nm, leading to a significant reduction in scattering efficiency.

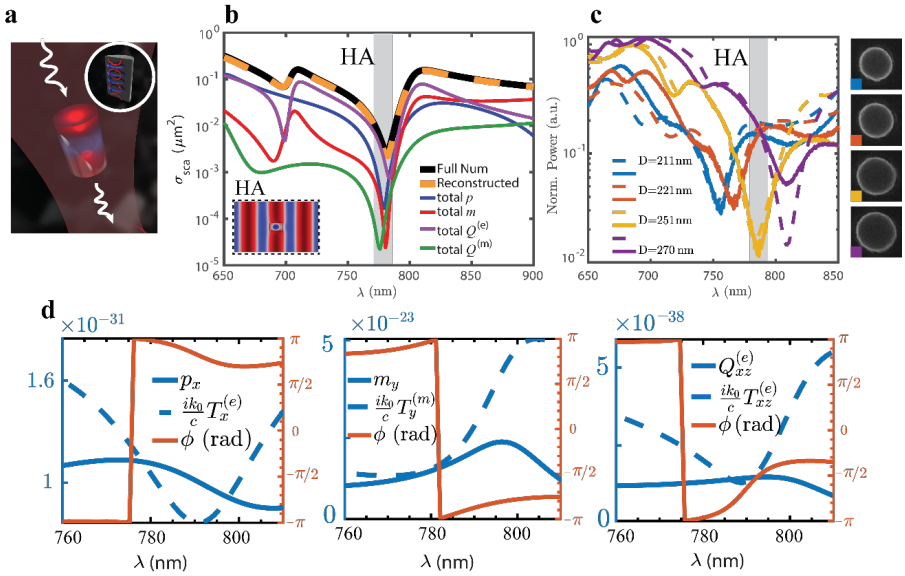

Fig. 1. Analysis of hybrid anapoles.

a – Artistic representation of the novel effect. **b** – Multipole reconstruction of the numerically obtained scattering cross section for the cylindrical amorphous silicon nanoparticle. **c** – The colored regions indicate the left plot: measured (solid lines) and simulated (dashed lines) scattering spectra of single isolated nanocylinders with different diameters *D*. The spectral positions of the hybrid anapoles. Right plot: SEM micrographs of the corresponding nanocylinder samples. The colored edges in each micrograph are associated with the measurements' legend entries. **d** – Amplitudes and phase differences between the multipoles and their toroidal counterparts. Panels from left to right, respectively: the basic electric and electric toroidal dipoles, the basic magnetic and magnetic toroidal dipoles, and the basic electric and electric toroidal quadrupoles. Amplitudes correspond to the left ordinate axis, and phase differences are read from the right ordinate axis.

Both HAs and EDAs suppress far-field radiation and enhance near-fields. However, HAs offer advantages over EDAs for nanophotonic applications. Figure 2 shows that EDAs exhibit poloidal-like field distributions and significant contributions from the magnetic quadrupole to radiation. This is a fundamental limitation of EDAs, as resonator modes with inversion symmetry will always radiate as combinations of multipoles with even or odd parity [47]–[48]. HAs, on the other hand, do not suffer from this limitation and can be designed to have purely electric dipole radiation, making them ideal for nanophotonic applications.

The complex multipole moments of the HA result in a unique internal field distribution, unlike the EDA (Fig. 2 b). This leads to a suppression of electric and magnetic dipoles and quadrupoles, significantly reducing scattering while maintaining a high local density of optical states (LDOS), as demonstrated by the calculations of the total electromagnetic energy stored within the two structures (Fig. 3 b). The stored energy in the HA is significantly higher than in the EDA, indicating enhanced light-matter interactions and nonlinear effects. Additionally, the HA modes exhibit larger quality factors.

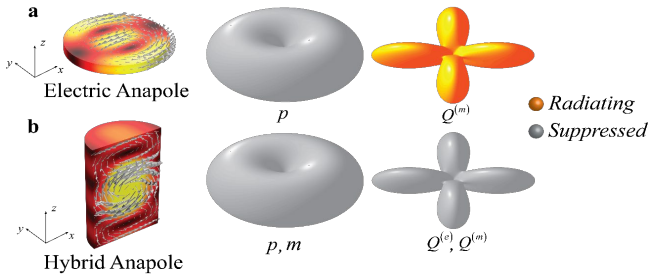

Fig. 2. Near and far-field characteristics of electric and hybrid anapoles.

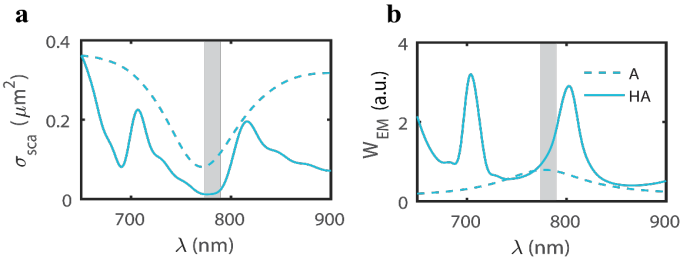

Fig. 3. Calculations of the total electromagnetic energy: radiated power (**a**) and stored electromagnetic energy (**b**) at the electric anapole (indicated by A) and the hybrid anapole (denoted with HA).

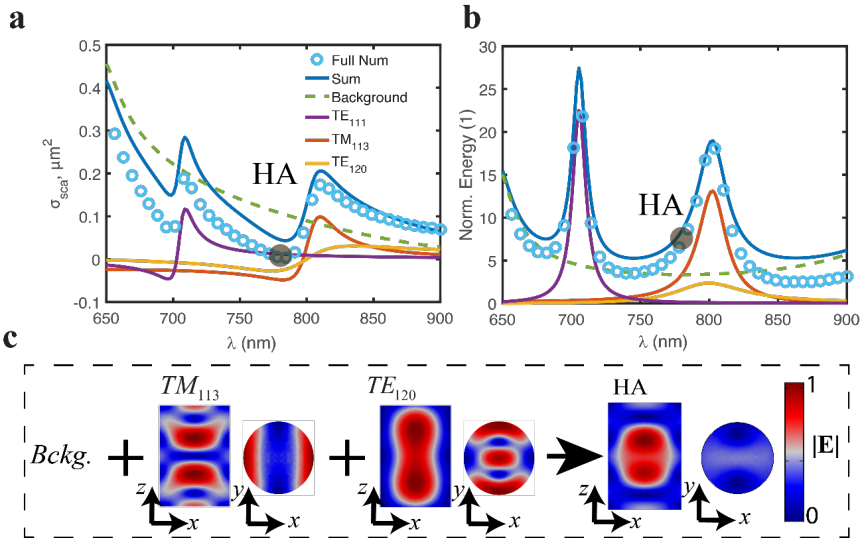

Fig. 4. Application of the QNM expansion method. **a** – Alternative scattering cross-section decomposition. Colored lines are the individual contributions of the physical QNMs. **b** – Spectra of the volume-averaged electromagnetic field energy inside the cylinder and the excited modes. **c** – Normalized internal electric field distributions.

It is important to emphasize the unusual feature of the hybrid anapole: the two resonant QNMs dominating the spectra are simultaneously negatively suppressed by interference with the background. A completely different picture emerges within the resonator. Figure 4 b

illustrates the modal decomposition of the internal energy stored in the cylinder near point HA. This is one of the main results of the section. Contrary to the multipole expansion, the QNM decomposition enables us to clearly distinguish the contributions of the eigenmodes to the internal fields. Firstly, we observe a significant enhancement of the electromagnetic energy (approximately nine times) compared to the incident plane wave. Secondly, it is clearly seen that the stored energy at the hybrid anapole is mainly driven by the TM113 mode due to its higher quality factor and the proximity of its resonant wavelength to the hybrid anapole wavelength, and to a lesser extent by the TE120 and the sum of the background contributions. Overall, the QNM analysis presented in Fig. 4 demonstrates that both the invisibility effect (outside the cylinder) and the internal energy enhancement at the HA are facilitated by the concurrent resonant response of the TM113 and the TE120 modes. On the other hand, the background modes, while they may not directly define the spectral features of the figures of merit, also play a crucial role. Their interference with the resonant modes leads to the invisibility effect. This interpretation is consistent with early investigations [49] regarding the formation of Fano lineshapes in the scattering cross-section of spherical resonators.

The QNM theoretical framework is highly suitable for quantitative investigations of nanoresonator dynamics under ultrashort pulses. As a result of this comprehensive research on hybrid anapoles, we have confirmed their existence in the stationary regime where destructive interference between electric and magnetic multipoles creates non-scattering zones. We have experimentally confirmed quadrupole anapoles and magnetic anapoles in subwavelength nanoparticles, which offer the potential for enhanced nonlinearities without scattering. Additionally, we have developed a physical model to understand the underlying eigenmodes that influence resonator response. This metasurface shows promise for applications in ultrafast dynamic nanophotonics, including temporal and spectral shaping of femtosecond laser pulses.

2.2. Nanoparticle dynamics in the optical nanovortex and its applications for lab-on-a-chip platforms

Nanophotonic approaches can enhance capabilities in microchambers and microreactors, which is essential for control over fluid flows at small scales in the field of microfluidics. This chapter focuses on the concept involving enhanced optically-driven diffusion and nanoparticle sorting utilizing high-index dielectric nanoantennas. Spin-orbit angular momentum transfer and radiation pressure create subwavelength optical nanovortices, enabling moving-part-free nanomixing and precise sorting of gold nanoparticles. This versatile platform enables miniaturized, optically driven microfluidic chips for chemical analysis, emulsion preparation, and light-controlled navigation of nanoparticles, viruses, or biomolecules.

Figure 5 presents a proposed nanomixing scheme: a silicon nanocube with refractive index $n = 4$ submerged in a water solution is illuminated by a circularly polarized laser beam from the top. The scattered field carries a non-zero tangential component of the Poynting vector in the x-y plane, which induces non-zero orbital angular momentum in the negative z-direction. The same effect causes the spiral motion of gold nanoparticles around the nanocube. Viscous friction between the moving nanoparticles and the fluid gives rise to convective fluid motion, enhancing

fluid mixing. Nanoparticles of different sizes, with opposite signs of the real part of polarizability, are radially displaced in opposite directions – the smaller ones move towards the nanocube, while the larger ones move away from it (Fig. 5 b). Since the nanostructure has negligible losses, the total angular momentum of the incident and scattered light is conserved. This conservation law for the total angular momentum implies that part of the incident SAM is transferred to both SAM and OAM of the scattered field, leading to spin-orbit coupling phenomena.

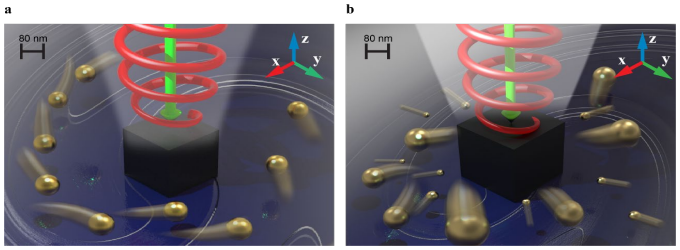

Fig. 5. An artistic view of the proposed active nanomixing scheme (a) and radial separation of nanoparticles (b).

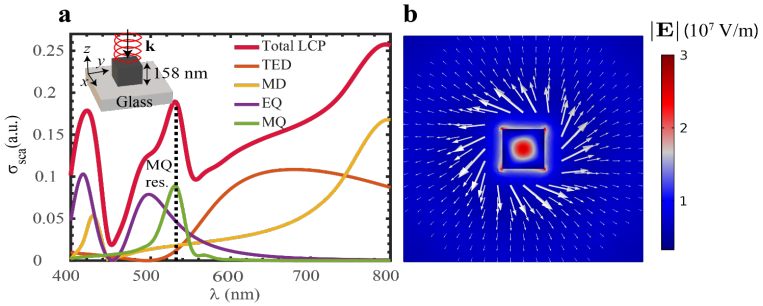

Fig. 6. Multipole decomposition for the scattering cross-section of the nanocube. **a** – The geometry is illustrated in the top inset, and the ambient medium is water. The dashed black line indicates the position of the resonant MQ mode (green laser, 532 nm). **b** – The color plot denotes the norm of the total electric field at 532 nm wavelength in the transverse x-y plane at z = 70 nm.

To characterize the trajectories of the nanoparticles inside the vortex and the enhancement of their diffusional motion, we calculated their mean-squared angular displacements (MSAD, $\langle \Delta\phi^2 \rangle$ in Fig. 8 a) with respect to the center of the nanocube.

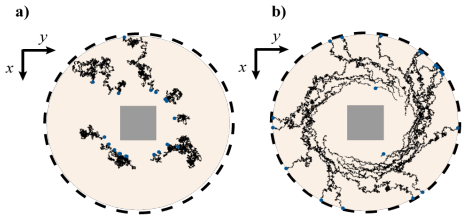

Fig. 7. Trajectories of Au nanoparticles of 40 nm radius during 1 ms of simulations. **a)** – No incident illumination, only Brownian motion and drag forces act on the particles. **b)** – The nanocube is illuminated with a circularly polarized light, and the optical force contributes significantly.

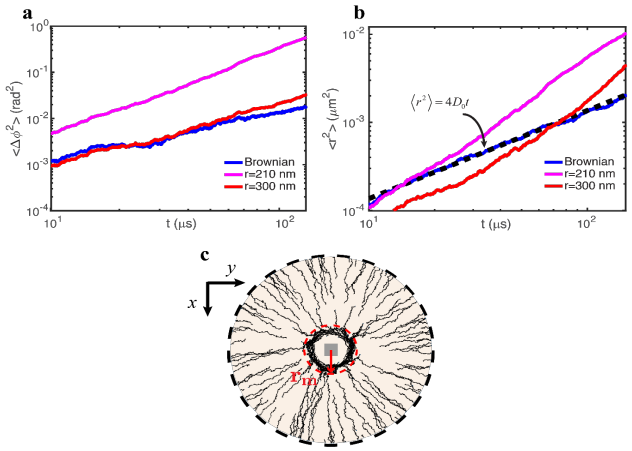

Fig. 8. Log-log plots of MSAD and MSD characterizing the diffusional motion of Au nanoparticles under the influence of the optical near fields. **a** – Calculated MSAD averaged over 100 Au nanoparticles of 40 nm radius when the cube is not illuminated (blue), and under LCP illumination at a distance from the center of the nanocube much lower than r_m (shown in **c**) – violet and at r_m – red. **b** – Averaged MSD in the same conditions as in **a**. Dashed line corresponds to the fit with Einstein's relation. **c** – Trajectories of 40 nm radius Au nanoparticles inside and outside the nanovortex region delimited by r_m.

The radius rm reaches about half of the incident wavelength in water. Therefore, the mechanical effect of optical vortices on a nanoparticle occurs in the subwavelength region. Such a reduced scale cannot be achieved using any focused far-field beams, such as radial and Bessel beams [50]–[52]. To our knowledge, this is the first proposal to provide optical nanovortices created in a simple, realizable setup, avoiding the need for lossy plasmonic nanoantennas [53]–[54], short-wavelength guided modes [55], or complex chiral structures [56]. Such optical nanovortices represent a promising component for on-chip orbital angular momentum (OAM) exchange, driving light-matter interactions such as controlled light emission from quantum dots [57], super-resolution [58]–[59], and manipulation of nanoobjects [60].

These effects enable us to demonstrate a novel, dynamic, contactless size sorting method for gold nanoparticles in liquid solutions, addressing one of the most challenging goals of conventional microfluidics with the assistance of dielectric nanophotonics. This demonstrates that our novel platform can operate as a sorting device for gold nanoparticles by exploiting their inward or outward motion towards the nanocube based on their dimensions. A precise, in-situ size control of gold nanoparticles is a crucial step in many applications, such as determining biological cell uptake rates [61], [62], toxicity [63], and Raman signal intensity [64].

2.3. Controlling ultrashort pulse propagation in disordered layered media

Optical nanostructures with loss and gain components are gaining attention as versatile materials for nanophotonic applications. In this chapter, a one-dimensional layered structure with resonant loss and gain is studied. The author modifies the typical loss-gain setting by introducing another variable into the system – disorder. Recently, it has been discovered that disordered metamaterials are of great interest not only because of Anderson localization [65],

[66] but also for observing topological state transitions [67], enhancing transmission [68], and shaping wavefronts [69]. Another feature that was considers is the emphasis on the dynamics of short pulse propagation. Therefore, the results belong not only to the fields of active and disordered photonics but also continue the long chain of investigations dedicated to coherent pulse propagation in resonant media [70]. In particular, the analysis is naturally connected to the studies of self-induced transparency (SIT) [71], [72] and related coherent effects such as the formation of population density gratings [73], [74] and collisions between solitonic pulses [75]–[77]. In this case, we are interested in systems with disorder in the parameters of the resonant part while the background remains uniform.

The system considered in this chapter consists of a background dielectric doped with active (two-level) atoms (Fig. 9). Light propagation in this medium can be described in the semiclassical approximation by the well-known Maxwell–Bloch equations. The model of disorder considered here implies that the initial population difference in the j^{th} layer of the medium corresponding to the distance $(j-1)\delta L < z \leq j\delta L$ is given by

$$w^{(j)}{}_0 = 1 - 2\xi_j r, \tag{1}$$

where ξ_j is the random number uniformly distributed in the range [0; 1] and r is the parameter of the disorder strength. When $r = 0$, we have the trivial case of purely absorbing (lossy) medium (all $w^{(j)}{}_0 = 1$). On the contrary, $r = 1$, corresponds to the maximal disorder, when loss and gain have equal probability to appear. In other words, the system can be considered as a multilayer (total thickness L) consisting of slabs (thickness δL) with different initial population differences, that is, different parts of the medium are under different pumping. For $r > 0.5$, the gain layers with $w^{(j)}{}_0 < 0$ become possible. Thus, the parameter r not only governs deviation from the ordered case of pure loss but also takes on the role of pumping strength, resulting in the appearance of gain. An example of distribution governed by Equation (5) is depicted in Fig. 10 for the period of random density variations $\delta L = \lambda/4$ and maximal disorder $r = 1$.

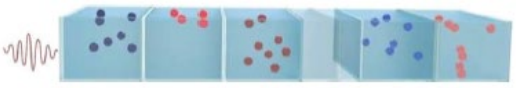

Fig. 9. Schematic depiction of the system under consideration. Different shades of blue and red denote different levels of loss and gain, respectively.

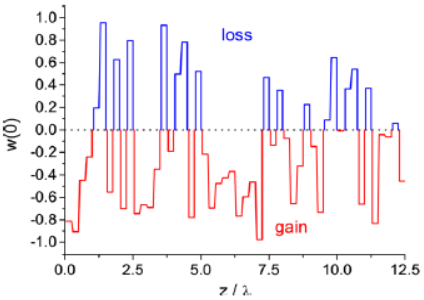

Fig. 10. Examples of initial population difference $w(0)$ distributed along the medium for the model of disorder.

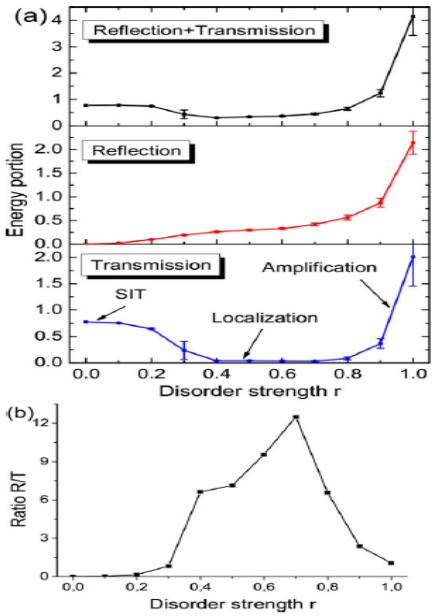

Fig. 11. Calculation of transmission and reflection for different levels of disorder. **(a)** – Average output energy of transmitted (bottom) and reflected (middle) light as well as their sum (top). Energy averaged over 100 realizations was calculated for the time interval 500 tp and was normalized on the input energy. The layer thickness is $\delta L = \lambda/4$. The error bars show the unbiased standard deviations for the corresponding average values. **(b)** – The ratio of average values of reflection and transmission as a function of *r*.

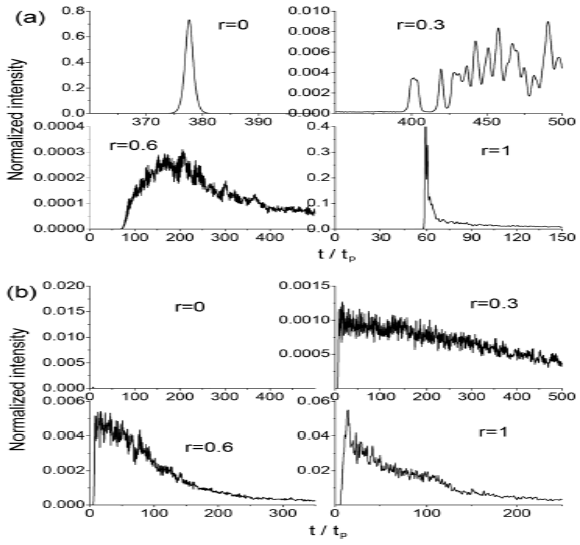

Fig. 12. Profiles of (a) transmitted and (b) reflected for different values of the disorder parameter *r*. Profiles are averaged over 100 realizations; the layer thickness is $\delta L = \lambda/4$.

Figure 11 (a) shows the mean values of transmission and reflection for different levels of disorder calculated within the modeled framework. At low disorder ($r \leq 0.2$), we have the SIT regime with high transmission, and the resulting pulse corresponds to a SIT soliton. As a result, a solitonic pulse of a specific form can be observed propagating through the medium with low attenuation. This is exactly what we see in Fig. 12 (a). For $r > 0.2$, the transition to localization occurs with a gradual decrease in transmission and an increase in reflection and absorption. In this scenario, trapping occurs closer to the entrance as the disorder increases. This results in the slowing down of SIT pulses and the observation of an almost standing population inversion for a realization with $r = 0.4$.

Overall, the propagation of ultrashort pulses was investigated in a resonant multilayered medium with randomly varying initial population differences along the propagation direction. The focus was on an active system with a disordered loss-gain distribution and a uniform background. As a result, three potential disorder models were considered, revealing two transitions and three distinct regimes as the disorder increased. The transitions were from the self-induced transparency (SIT) regime to the localization regime and then to the amplification regime. The amplification regime only appeared when negative population differences were possible and the disorder was sufficiently large. These effects offer opportunities for flexible control over the optical response of the medium, allowing for adjustments in the reflection-to-transmission ratio and pulse propagation speed through the disorder parameter.

2.4. Analysis of the diffusion-inspired emission dynamics in nanostructured environments

In the study of light-matter interaction, the structured environment controls the dynamics by modifying the local density of electromagnetic states. While fast fluorescent processes may overlook mechanical changes, slow-decaying phosphorescent complexes can detect micro- and millisecond-scale motion through near-field interactions. By examining the interplay between time-varying Purcell enhancement and molecular motion, we analyze collective decay phenomena using a modified diffusion equation. Mapping fluid properties onto phosphorescent lifetime distribution enables contactless all-optical thermometry and diffusion measurements. This photonic platform has potential applications in nanofluidic processes and lab-on-a-chip (LOCP) devices, offering insights that are challenging to acquire with other optical methods.

This chapter presents a theoretical framework for analyzing diffusion processes of slow-decaying phosphorescent compounds in a solution of resonant optical antennas (see Fig. 13). An assembly of emitters dissolved in a liquid mixed with metal nanoparticles is pumped with external illumination. Slow-decaying dyes diffuse in the vicinity of resonating nanoparticles, which change their emission on a timescale comparable to spontaneous decay. As a result of this interaction, the information on fluid dynamics is imprinted in the photon statistics.

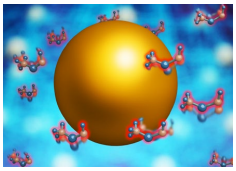

Fig. 13. The schematics of the system – diffusion of slow-decaying phosphorescent dyes next to a resonating nanoantenna.

Radiative and nonradiative enhancements should be distinguished because they influence the interaction between light and matter in different ways. The total radiative lifetime governs the decay dynamics, while the radiative contribution is responsible for the number of photons detected at the far field. The difference between radiative and total rates is the result of losses within the particle. While in the majority of optoelectronic applications, only the radiative enhancement is a factor for maximization, the presented diffusion model requires knowledge of the total decay rate. The information about the local properties of the fluid, however, can be analyzed by collecting emitted photons. The following typical parameters have been used: the radius of the spherical particle is 50 nm, and the optical properties of gold were taken from [95]. The central wavelength of phosphorescent emission is 690 nm.

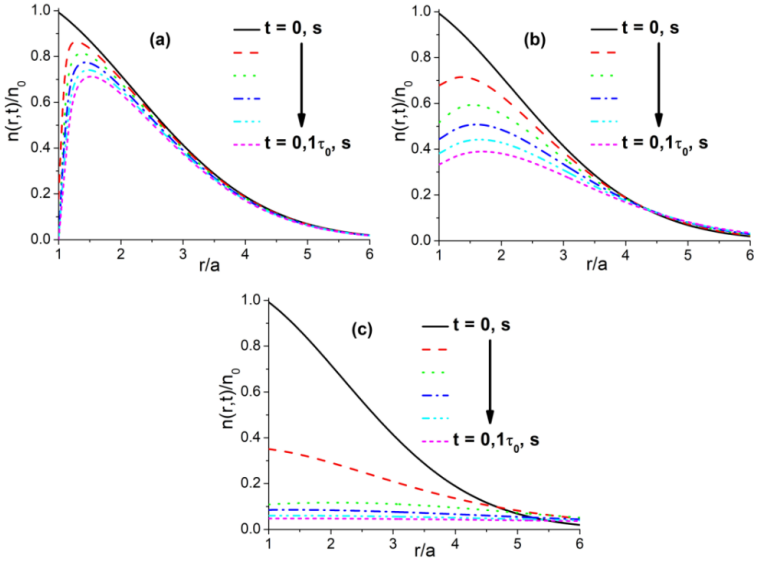

Fig. 14. Radial distribution of excited dye molecules in the vicinity of the particle at different times for different diffusion coefficient values: (a) – 0; (b) – 0.2; (c) – 1.6.

It can be seen from Fig. 14 that when the diffusion coefficient is very small, the population of excited dyes drops rapidly near the particle, and there is no Brownian inflow towards it. On the other hand, when diffusion is efficient, slow-decaying molecules (unaffected by Purcell enhancement) flow in and begin to sense the presence of the antenna. As a result, they decay

faster. This dynamic behavior is clearly observed by comparing panels a, b, and c. The decay kinetics directly affect the lifetime distribution, which can be measured in the far-field.

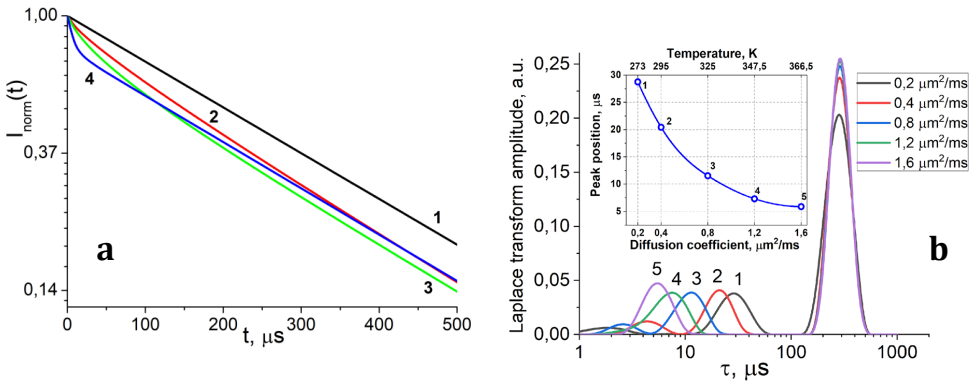

Fig. 15. **a** – Normalized intensity (log-scale) decay of the dye molecules in the vicinity of the particle for different diffusion coefficient values. **b** – Lifetime distribution analysis of the collected luminescence signal.

Fig. 15 a demonstrates the time-dependent intensity decay for various values of the diffusion constant. When the molecules are randomly moving around the antenna, they have a higher probability of being found in its vicinity, leading to a larger Purcell enhancement. This result is illustrated in Fig. 15 b, where the non-exponential response of the system is clearly visible. The rightmost peak corresponds to the free-space relaxation time of the molecules. The secondary peak on the left is associated with the Purcell effect and contains information about the diffusion characteristics. Indeed, the increase in the diffusion coefficient leads to a further shift of this secondary peak towards shorter lifetimes. This shift occurs because there is an increasing probability for molecules to approach the metal nanoparticle. The position of this peak as a function of the diffusion coefficient and, consequently, the temperature is shown in the inset. Therefore, it becomes possible to measure temperature and diffusion coefficient in a liquid using the proposed photonic contactless design. The pronounced dependence of the optical signature of phosphorescent molecules on their surroundings can be extremely useful in various applications such as microfluidics and microchamber-based chemistry, remote all-optical temperature control, microbiology, and biomedicine.

2.5. Modeling optical binding effect in hyperbolic metamaterials

This chapter discusses the capabilities of hyperbolic metamaterial substrates for optical binding applications. A typical scenario is depicted in Fig. 16, where a pair of small particles are linked together by an optical field, mediated by a structured surface.

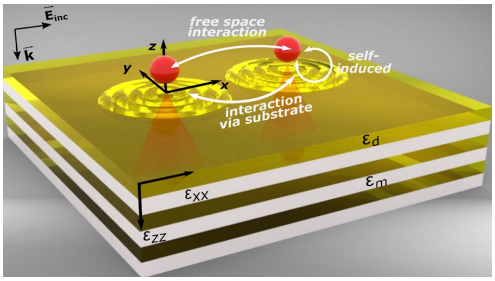

Fig. 16. The general concept of optical binding above a metamaterial slab. Highly confined optical modes within the layered hyperbolic metamaterial create additional interaction channels, enabling the formation of dimers and chains with separation distances smaller than the diffraction limit.

Figure 17 shows the resulting optical forces corresponding to the dominant contributions of SPPs and hyperbolic modes. In the first case, optical forces are primarily influenced by the strong impact of surface plasmon-polaritons, with these surface waves fully driving the forces, while the contribution of other modes is inadequate. In the latter case, where hyperbolic modes have the predominant influence, optical binding has almost nothing special compared to the free-space scenario. Here, HMs contribution increases the force by almost twice (which is still two orders of magnitude less than that of SPPs) and slightly shifts equilibrium positions, almost not affecting L_{bind} . Thus, hyperbolic modes excited by the first particle propagate symmetrically in the volume without interacting with the second particle, and vice versa. However, the still existing nonzero contribution of HMs can be explained through the aforementioned cross-terms. In this scenario, modes excited by one particle are scattered by another, resulting in additional HMs with broken symmetry. These, in turn, contribute to the optical force shift [96].

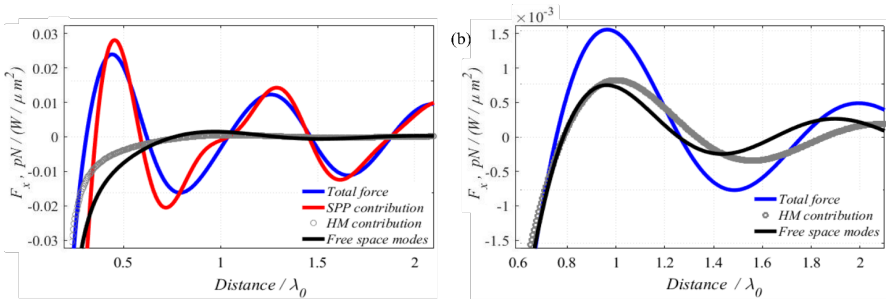

Fig. 17. Dependence of the optical binding force on the distance between the particles: (a) SPPs, (b) hyperbolic modes.

Therefore, it demonstrates that hyperbolic modes, even though dominant in the interaction with the semi-infinite metamaterial, do not provide a sufficient contribution to binding in this case. The main reason for the weak influence of HMs on binding is the absence of feedback from the bulk modes, which propagate away from the particles to infinity. However, strong optical binding can be achieved by using an anisotropic finite thickness slab because of the

reflections of hyperbolic modes from the boundaries. The structure under consideration is shown in Fig. 18.

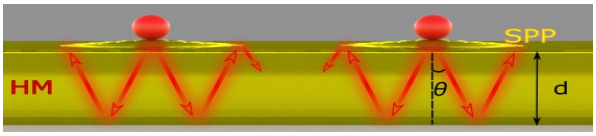

Fig. 18. The scheme of optical binding near anisotropic hyperbolic metamaterial (HM) slab. Reflections from the boundaries of the slab form high-intensity regions and result in optical binding with separation distances L_{bind} below the diffraction limit.

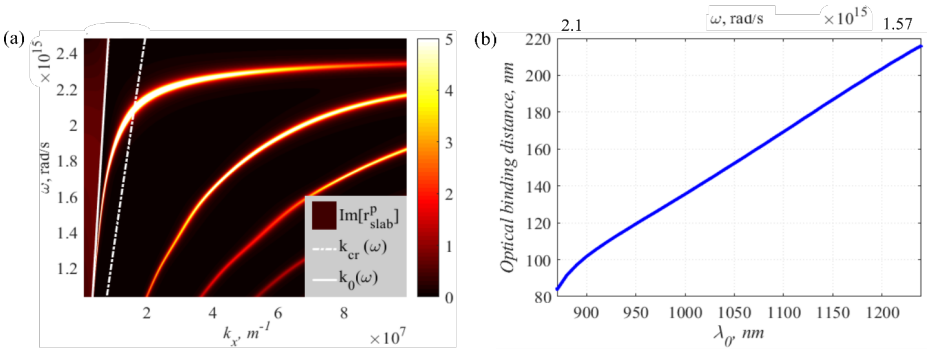

Fig. 19. Chromatic tuning for the multilayered structure of silver and Ta_2O_5 layers with a slab thickness 115 nm and filling factor of 0.133. (a) – Imaginary part of the reflection coefficient (dispersion diagram). (b) – Optical binding period over the frequency.

Additionally, we can consider another important degree of freedom – chromatic tuning of the metamaterial-assisted optical binding. Figure 19 (a) shows the dependence of the reflection coefficient on the incident wave frequency for a slab thickness of 115 nm. It can be seen that the number of HM peaks controlled by the reflections (similar to Fabry–Perot resonances for hyperbolic modes) and contributing to optical binding increases with lower frequency. Therefore, the dependence of optical force becomes more complex. The distance between the bound particles (Fig. 19 (b)) now varies with frequency, highlighting the significant role of material dispersion in this context. The binding period is proportional to the ratio of the thickness of the slab and the incident wavelength. In this case, the permittivities are monotonically dependent on the frequency; thus, the optical binding distance's dependence is more or less monotonous. However, in other wavelength regions, additional heavy metals (HMs) and non-monotonic dispersion of optical constants could displace the stable equilibrium positions and alter the relationship depicted in Fig. 19 (b). This additional degree of freedom opens up a realm of opportunities for tuning optical binding in a "non-invasive" manner and fabricating novel designs and architectures of nanostructures on metamaterial substrates by adjusting optically induced forces with hyperbolic modes.

2.6. Modeling superscattering effect emerging from the physics of bound states in the continuum

This chapter studies the Mie-like scattering from an open subwavelength resonator made of a high-index dielectric material when its parameters are tuned to the regime of interfering resonances. We have discovered a novel mechanism of superscattering, closely linked to the strong coupling of resonant modes [99] and described by the physics of bound states in the continuum (BICs). We demonstrate that the enhanced scattering occurs due to constructive interference described by the Friedrich–Wintgen mechanism of interfering resonances [100], which allows the scattering cross-section of a multipole resonance to exceed the currently established limit. Here, we develop a comprehensive non-Hermitian model to describe the interference of resonances of quasi-normal modes.

Figure 20 (a) illustrates a proposed concept of the superscattering effect inspired by BIC in an isolated resonator. Mode coupling induces power redistribution within two radiation channels, enabling the overcoming of the single-channel scattering limit. This process allows for the control of not only the Q-factor but also the enhancement of the power scattered by a multipole (e.g., the electric dipole) beyond the limit, as demonstrated in Fig. 20 (b).

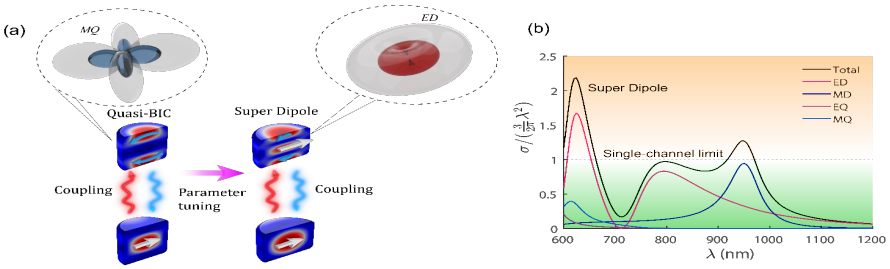

Fig. 20. (a) – Concept of BIC-inspired superscattering in an isolated resonator. (b) – Super dipole resonance arising in the scattering cross-section of a dielectric cylinder with refractive index $n = 3.8$, radius 130 nm, and height 180 nm.

The scattering cross-section of the electric dipole channel significantly exceeds the single-channel limit. This is in contrast with conventional superscattering, where several multipole resonances need to be overlapped.

To design a superscatterer, the resonant frequencies of several quasi-normal modes (QNMs) associated with different multipolar channels must be brought together through a specific design of the particle geometry. This design aims to ensure that the total scattering cross-section, which is the sum of their contributions, surpasses the limit. Moreover, depending on the symmetry of the object, the scattering cross-section of one multipole can receive contributions from other multipoles. This suggests that the strength of a multipole could, in theory, be boosted beyond the conventionally accepted limit.

To illustrate super-multipoles emerging from quasi-BICs, we extend our TCMT model to the case of a structure supporting two QNMs, each compatible with a single scattering channel. In order to model a subwavelength nanoresonator, let us consider a silicon nanosphere in air

illuminated by a normally incident, linearly polarized plane wave with a radius of 100 nm. In the visible range, there are two quasi-normal modes (QNMs) that correspond to the electric dipole (ED) and magnetic quadrupole (MQ) channels, respectively. The electric field distributions are depicted in the lower panel of Fig. 21 ©. Note that the selected scatterer is significantly subwavelength, with a radius at least five times smaller than the incident wavelength.

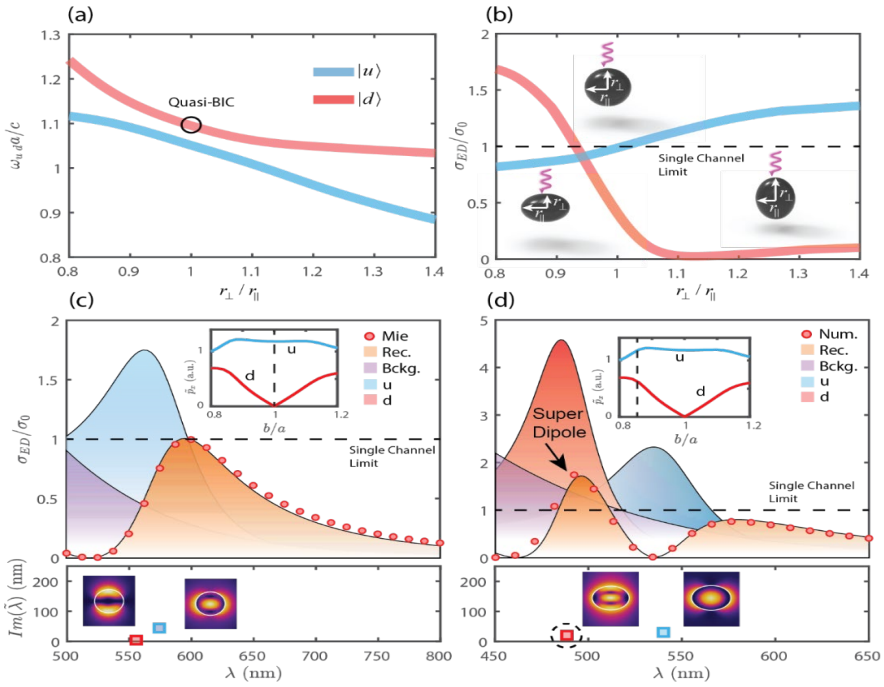

Fig. 21. (a) – Evolution of the resonant frequencies of the ED and MQ modes of a silicon nanosphere (100 nm radius) when breaking the rotational symmetry along one of its axes. (b) – Scattering cross-section of the ED channel at the two resonance maxima as a function of ellipticity, under normally incident, linearly polarized plane wave illumination, with momentum oriented along the axis with broken rotational symmetry. (c) and (d) – Contributions of the QNMs to the scattering cross-section of the ED channel in a sphere and a perturbed spheroid.

In order to couple both QNMs, it is necessary to break the spherical symmetry in some fashion. A simple way to do so is by reducing the rotational symmetry in the plane parallel to the direction of propagation (see schematic insets in Fig. 21 (b)). In this case, multipolar modes with the same parity (as in the case of the chosen QNMs) can couple [101]. We gain insight into the mechanism by evaluating the influence of each QNM on the ED scattering cross-section (Fig. 21 (c)–(d). The reconstruction is in excellent agreement with the exact analytical results of Mie theory for the sphere (Fig. 21 (c)) and full-wave numerical simulations for the ellipsoid (Fig. 21 (d)). It is important to note that the “direct” cross-section of each QNM, by itself, is not bound by any limit.

This example illustrates the formation of a super dipole resulting from a symmetry-breaking perturbation. However, spheroids are generally not easy to fabricate at the nanoscale. Instead, we can also achieve this regime similarly in a silicon nanorod under normally incident illumination (Fig. 22 (a)), as the latter also possesses cylindrical symmetry. To do so, we perturb the height of the resonator by an amount of Δh, starting from a height of $h_0 = 180$ nm, for which two modes radiating ED and MQ, are spectrally close. In the spheroid, we observe a system of two coupled resonant quasi-normal modes (QNMs) with relatively high Q-factors.

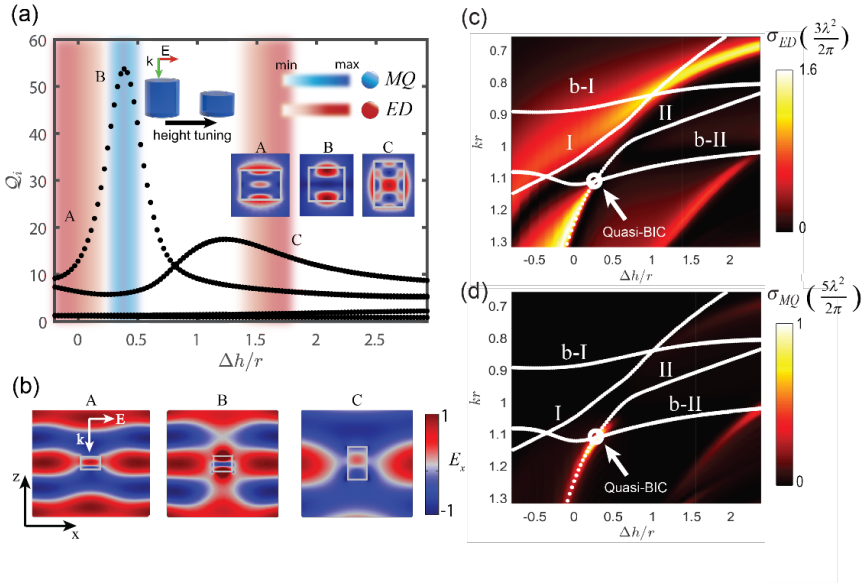

Fig. 22. Design of a super dipole mode in a Si nanorod. (a) – Quality factors and multipolar radiation of the QNMs as a function of a perturbation of the cylinder height Δh, normalized by the radius r = 130 nm. (b) – E_X component of the total field at the superscattering points A-C indicated in (a), under x-polarized plane wave illumination (in arbitrary units). (c)–(d) – 2D maps of the ED and MQ scattering cross-sections as a function of kr and $\Delta h/r$.

Next, we conducted a proof-of-concept experiment by measuring the extinction cross-section and scattering patterns of disk-shaped resonators in the microwave range. We replicated the geometrical parameters of the rod by utilizing a set of ceramic resonators with fixed 4.0 mm radii and permittivity ε = 22 with a loss tangent of 0.001. As shown in the inset of Fig. 23 b, three samples are assembled from multiple disks to achieve the desired aspect ratios for the resonators. The measurement results of both the total extinction cross-section and electric near-field patterns are presented in Fig. 23. The spectra are normalized based on the ED single-channel limit. The experimental measurements are in reasonable agreement with the numerical simulations, although the resonances appear suppressed due to material losses in the ceramic. Since the resonances redshift with increasing size, the observations were performed over a wide frequency range. In the highlighted frequencies in Figs. 23 a and 23 c, we observe wide resonances with large extinction values, characteristic of the proposed super dipole modes.

Indeed, the plane wave is strongly distorted in the near field. Furthermore, numerical calculations confirm that the ED exceeds its limit, even when considering losses. The quasi-BIC appears at the expected value of $\Delta h/r = 0.48$, manifesting itself as a sharp peak in the spectra (Fig. 23 b). The results provide experimental evidence of controlling both the Q-factor and scattered power between two resonances to achieve the superscattering regime with just a single mode.

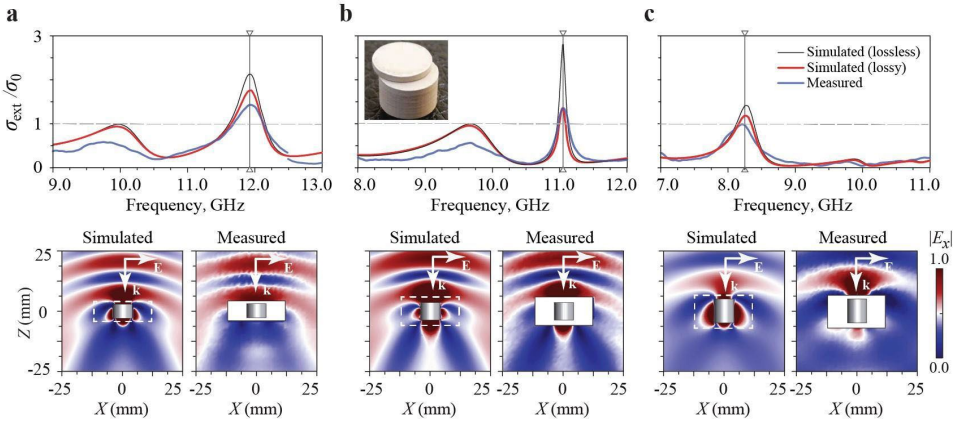

Fig. 23. Simulated and measured total extinction cross-sections and scattered electric near-field patterns. All the cross-sections are normalized by the single channel limit for the ED. Insets show an example of the experimental resonator and the electric field norms in the x-z plane of the resonances indicated by vertical lines in the top plots. The white regions in the near-field patterns correspond to the physically inaccessible zones for the measurements. The aspect ratios of the disks are: (a) $\Delta h/r = 0.25$, (b) $\Delta h/r = 0.475$, and (c) $\Delta h/r = 1.25$.

Novel superscattering regimes were demonstrated by utilizing subwavelength, nonspherical resonators and exploiting the strong coupling of two resonances. The findings show superscattering originating from an electric super dipole moment, surpassing the currently established limit by almost two times. By disrupting the quasi-BIC condition in resonators without spherical symmetry through parameter adjustments, power exchange between scattering channels enables the manipulation of Q-factors and multipolar contents while maintaining a high scattering cross-section. Our super multipole resonances exhibit enhanced resistance to ohmic losses compared to conventional counterparts. These findings have implications in biosensing [102], [103], energy harvesting [104]–[106], on-chip circuitry [107] and optical manipulation [108]–[109].

2.7. Optical properties of magnetic octupole in silicon quadrumers

The development of new approaches to tuning the resonant magnetic response of simple all-dielectric nanostructures is crucial in modern nanophotonics. This chapter demonstrates that a resonant magnetic octupole (MOCT) response can be achieved by dividing a solid rectangular silicon block into a quadrumer structure with the introduction of narrow gaps between four

nanocubes. We learn how to use controllable resonant MOCT excitation to tailor magnetic hotspots and resonant energy absorption.

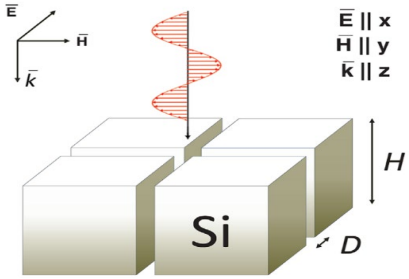

Fig. 24. The artistic representation of the quadrumer of silicon cubes.

The systems under consideration include a silicon block measuring 500 × 500 × 250 nm, representing the zero distance between silicon cubes in Fig. 24, and silicon quadrumers composed of four Si cubes (250 × 250 × 250 nm) with distances between them of D = 25 nm, 50 nm, and 100 nm. Material data for silicon has been taken from the reference [110]. To investigate spectral resonances in scattering cross-sections, we apply the multipole decomposition technique, which demonstrates good performance in all cases considered (Figs. 25–27).

It is possible to exploit this effect to design magnetic switchers at the nanoscale. It is important to go into detail with the physics of the considered process. Figures 26 a, c show the absolute value of the x-component of the electric field (Ex) in the solid block and in the quadrumer, respectively. Following Maxwell's equations, in the oligomer structure, the electric field enhancement appears in the slits along the polarization of the incident wave due to the discontinuity of the normal component. In addition, Figs. 26 b, d show the absolute value of the y-component of the magnetic field (Hy) and the crucial redistribution of the magnetic field because of the structuring. This leads to six different field concentration zones in the quadrumer structure, constructing a magnetic octupole nearfield pattern. The magnetic field does not undergo a discontinuity in the gaps along Hy (μ = 1 in both media), which is why the magnetic hot-spots take place between the cubes, too. In addition to the magnetic field enhancement, MOCT resonance can provide strong electromagnetic absorption in the quadrumer. Figure 26 a shows the comparison of absorbed power for λ between 850 nm and 900 nm for the solid silicon block and the quadrumer with the distance D = 25 nm between the cubes. Figure 26 b proves that the discovered energy absorption peak spectrally corresponds to the MOCT resonance. It is worth noting that in this spectral range, natural light absorption by silicon is small. Therefore, air gaps in the quadrumer structure cause strong absorption in silicon, despite its very small Im(n) ≈ 0.08. Figure 26 c compares the electric field inside the silicon block and quadrumer structure. Clearly, the resonant magnetic octupole response leads to a strong electric field concentration and, therefore, to the resonant absorption in the silicon quadrumer. The spectral position of the MOCT resonance and, hence, the position of the absorption peak can be changed

by varying the distance between the cubes. Such tunable absorption can be widely used to control the energy concentration by dielectric structures and to design modern optical devices.

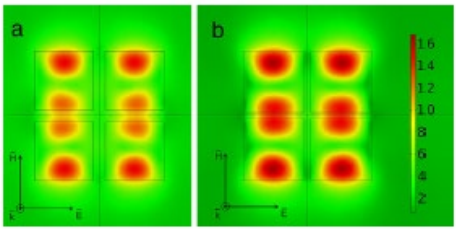

Fig. 25. Distribution of the normalized magnetic field in x-y- plane (z = 0) of the silicon quadrumer with a) D = 50 nm, λ = 863 nm; b) D = 25 nm, λ = 874 nm. The color bar is the same for both pictures.

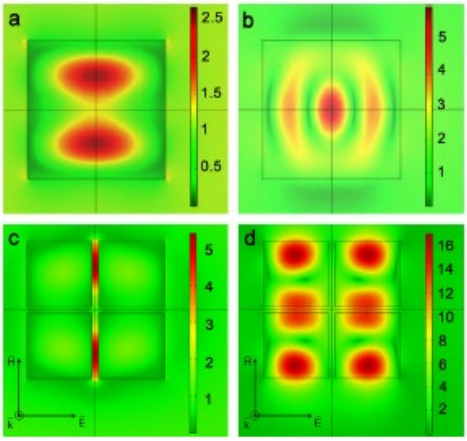

Fig. 26. The absolute value of Ex (a, c) and Hy (b, d) in the solid silicon block (a, b) and the silicon quadrumer (c, d) with D = 25 nm at λ = 874 nm.

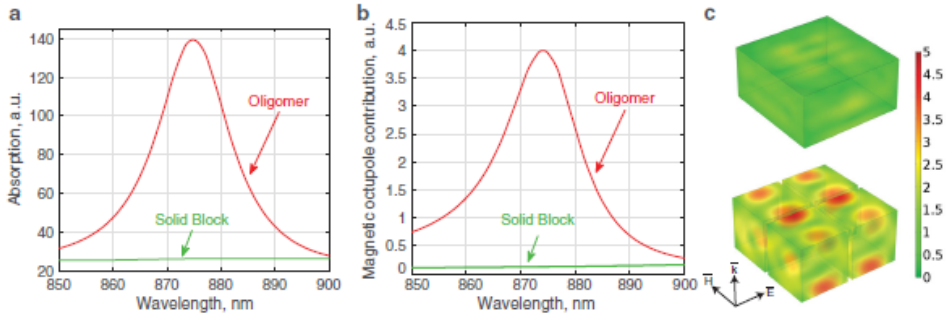

Fig. 27. Spectra of a) absorption power and b) MOCT contribution to the scattering cross section calculated for a single silicon block of height H = 250 nm and base edge 500 nm (green lines) and the quadrumer of silicon cubes with the distance between cubes D = 25 nm (red lines). The absorption peak in the structure clearly corresponds to the resonant excitation of the MOCT moment. c – Normalized electric field inside the solid block (top) and quadrumer (bottom) at λ = 874 nm. One can see that resonant MOCT response provides strong electric field concentration leading to the resonant absorption in the silicon quadrumer.

3. REAL-WORLD APPLICATIONS AND EXPERIMENTAL RESULTS

3.1. Macroporous phononic crystal-based structures for FBAR applications

This chapter investigates the most optimal solutions for the periodic structure design considering the technological aspects of the structure fabrication. The study was performed with the help of finite element method using COMSOL Multiphysics FEM software. The prime requirement is that the periodic structure should exhibit the existence of bandgaps at several frequency regions of the switchable FBAR. The current work is focused on the consideration of periodic structure designs that are technologically achievable for sub-micrometer dimensions using standard microfabrication approaches. With regard to that, the application of macroporous structures is proposed. Macroporous silicon-based structures can be fabricated utilizing standard masked electrochemical etching with the structure design that is predetermined by the photolithography.

In the current work the author found optimal solutions for pore arrangements of different symmetries that are completed as arrays of air-filled cylindrical inclusions in the silicon host material. 2D square, triangular and honeycomb arrangements of holes were used for this study, as shown in Fig. 28.

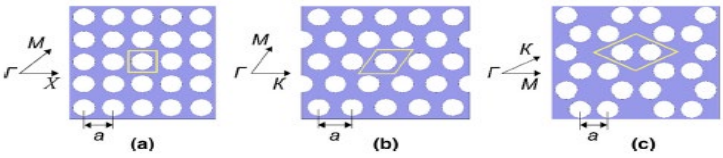

Fig. 28. Square (a), triangular (b), and honeycomb (c) arrangements of cylindrical holes in the silicon host material and propagation directions for 2D phononic crystals.

The silicon-based porous artificial periodic structures were modeled as arrays of air-filled cylinders for three different symmetry cases. This arrangement is obtained by translating the unit cells for each case, as shown in Fig. 28. The cylinders are assumed to be parallel to the z-axis; thus, in this study, we only consider the elastic waves that propagate in the x-y plane. For square 2D structures, the irreducible Brillouin zone spans from C to X to M and back to C. The results of the band diagram computation for the infinite periodic arrangement with a lattice constant of 0.94 μm, square symmetry, and a hole-filling factor of 76 % are demonstrated in Fig. 29 a. The filling factor is defined as the percentage ratio of the area of the holes per unit cell square. The dependence of absolute bandgap boundaries on the filling factor is demonstrated in Fig. 29 (b).

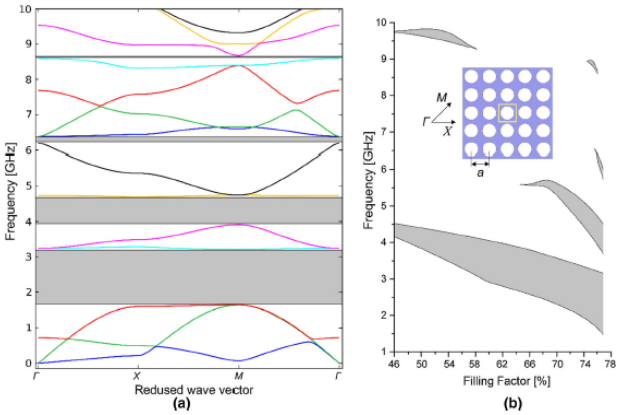

Fig. 29. Band diagram for the pore silicon infinite square arrangement, filling factor 76 % (a), and the dependence of the width of the absolute bandgaps from the filling factor (b) for a fixed value of lattice constant of 0.94 um.

As demonstrated in Fig. 29 (b), computational results show variations in bandgaps depending on the filling factor. The results indicate that increasing the diameter of the holes for the same lattice constant leads to a broadening of the low-frequency bandgap and the emergence of higher-frequency stop bands. At the same time, it can be seen that a relatively narrow high-frequency bandgap, which is found for low-filling factors, completely vanishes with an increase in the diameter of the holes. It should be mentioned that at a relatively high filling factor, the square symmetry arrangement exhibits a broad complete bandgap in the lower frequency range and a narrower bandgap at higher frequencies, which is advantageous for switchable FBAR applications. The displacement distribution and the analysis of frequency dependence of the structural reflection for the shear component of displacement are demonstrated in Fig. 30. In comparison to a complete FBAR structure, the simulation model should be extended to include top and bottom electrodes with a piezoelectric film in between. However, in order to simplify the calculations and obtain the results that determine the behavior of the periodic structure separately from the piezoelectric film, the model was reduced to the prescribed shear displacement at the boundary of the presumed FBAR reflector. In contrast to the simplified model, the finite FBAR structure will be expanded by incorporating a piezoelectric layer and electrodes of specific dimensions.

The computational results of triangular arrangement demonstrate the possibility of achieving several relatively narrow bandgaps at a high filling factor. From a practical standpoint, that arrangement is not optimal because the achievable bandgaps are relatively narrow for applications requiring multiple operation bands and support frequency switching within very limited regions.

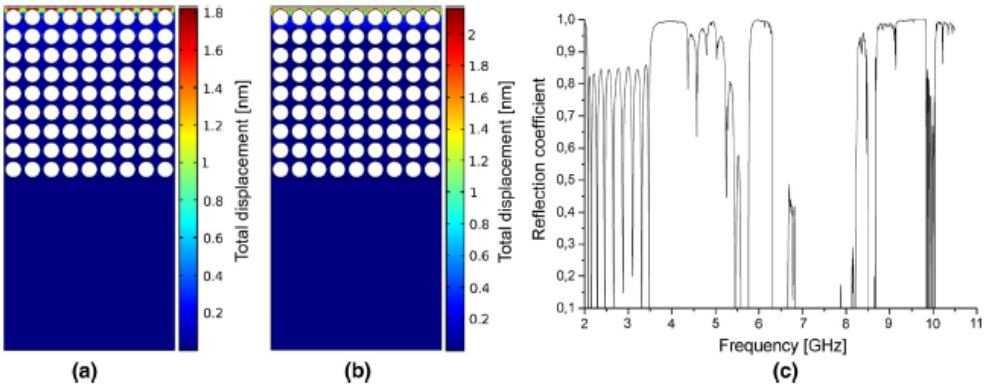

Fig. 30. Simulation results of square arrangement of air-filled cylinders in the silicon matrix (filling factor 54 %). Displacement distribution of the structure excited with a shear displacement applied to the top structure boundary taken at frequencies of 4 GHz (a) and 9.5 GHz (b), and the structure reflection coefficient.

The obtained results show that increasing the structure's wavelength shifts the bandgaps towards lower frequency regions, as expected. In this current contribution, we have presented the results of theoretical research focused on studying technologically competitive solutions of phononic structures for enhancing the performance of FBAR devices. We propose considering the established technological platform for fabricating macroporous structures as an approach that enables the realization of phononic-based acoustic reflectors for FBAR SMR devices and studying appropriate periodic structure solutions using numerical methods. It was found that the honeycomb arrangement is the most advantageous in terms of bandgap performance, which should allow the FBAR structures to operate within a broad frequency range. The completed work represents an initial step towards the fabrication of photonic crystal-based FBAR devices.

3.2. Modeling and characterization of microspheres with silver molecular clusters for sensor applications

This subchapter explores silver-molecular-cluster-containing microspheres for advanced sensors. These microspheres are synthesized through an ion exchange process with silver nitrate and sodium nitrate, creating unique optical properties. A simulation shows an enhanced radiation interaction due to extended fundamental mode propagation. This study investigates luminescence in the visible range (400–600 nm) when excited by long-wavelength UV light (360–410 nm), offering the potential for sensing applications. These microspheres find use in environmental sensing (pollutant detection), biomedicine (drug delivery, bioimaging), and industrial process monitoring.

To create the silicate glass microspheres, glass was employed. The production process involved several steps. Initially, a thin fiber was crafted, and subsequently, the microspheres were formed by melting the fiber’s end using a propane flame. The microspheres were then subjected to the low-temperature ion exchange (LTIE) process.

Figure 31 displays photographs of the samples obtained. Notably, the smallest sample achievable through the described method had a diameter of 200 microns.

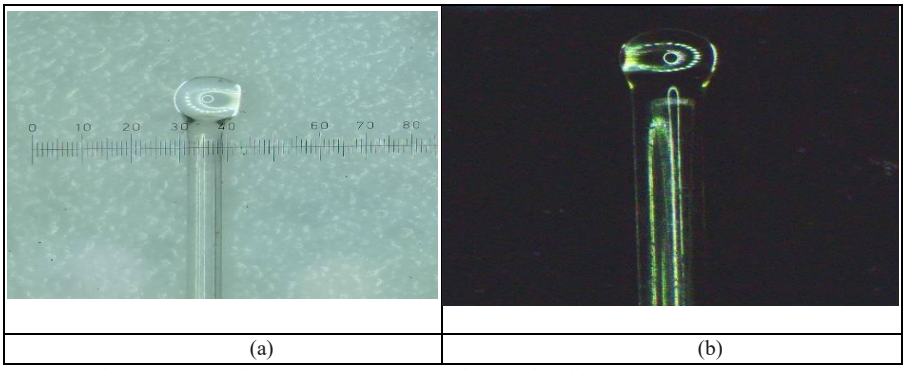

Fig. 31. The obtained microsphere samples: (a) microsphere with a diameter of 380 μm; (b) microsphere with a diameter of 200 μm.

COMSOL Multiphysics was employed to determine the resonant frequencies and fundamental modes of the resonator. The investigation of the properties of silicate glass containing silver molecular clusters, synthesized through the LTIE method, encompassed both absorption measurements and luminescence spectra measurements. Absorbance measurements were conducted on the witness samples using a UV-VIS spectrophotometer (PB 2201). Luminescence spectral acquisition measurements were performed using a Fluorolog®-3 instrument with FluorEssence™ (Manufacturer: HORIBA Jobin Yvon SAS, France). For all luminescence measurements, the integration time was 0.1 s.

An experiment was conducted to measure the absorption of glass samples that underwent low-temperature ion exchange (LTIE), as well as transparent glass samples that were not subjected to LTIE treatment. The resulting spectrum is depicted in Fig. 32. Notably, the absorption spectrum of the samples after the LTIE process lacks characteristic absorption peaks. This absence is attributed to the fact that, under the same process parameters used in the treatment, predominantly silver molecular clusters, such as Ag2...5, are formed [111].

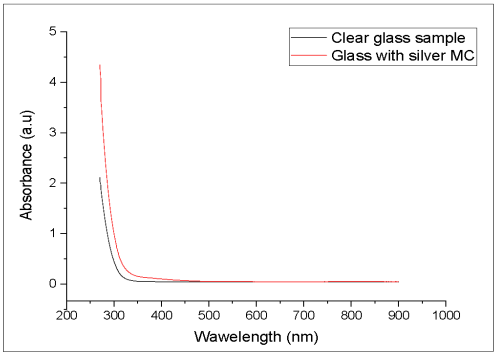

Fig. 32. Measured absorption spectra of glass samples.

Figure 33 presents the results of measuring the luminescence intensity. When excited at wavelengths of 370 nm and 390 nm, the luminescence spectra of all synthesized glasses exhibit a broad luminescence band within the visible spectrum. This broadband luminescence spanning from 500 nm to 900 nm corresponds to the emission emanating from a small quantity of silver microcrystals formed directly during the LTIE process [112]. To generate molecular clusters (MC), it is imperative to reduce silver ions to their atomic state. This transformation leads to the creation of a certain quantity of silver microcrystals during the LTIE process, consequently giving rise to weak luminescence across the entire visible range.

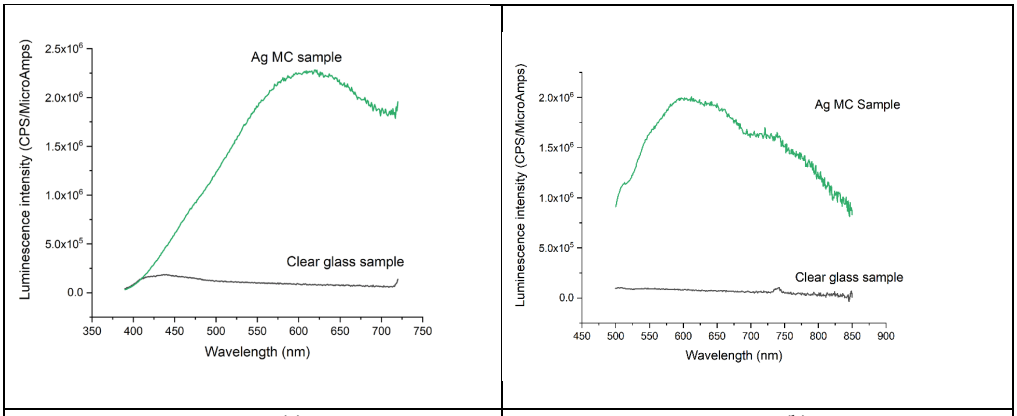

(a) (b)

Fig. 33. Luminescence intensity: (a) first sample, λ_{exc} 370 nm; (b) second sample, λ_{exc} 390 nm.

The simulated microspheres had a radius of 100 μm. During the LTIE process with silver, the glass changes its refractive index from 1.585 at the surface to 1.515. The simulated microsphere had a gradient refractive index from the edge to the center. To explore the potential of this material, simulations of microspheres in air and water were conducted. Figure 34 shows the distribution of the electromagnetic field in the cross-section of the microcavity in air (a) and water (b). The resonant wavelength for the fundamental mode of the microresonator near the luminescence peak was determined. For a microsphere in air, the resonant wavelength for the fundamental TE mode with an azimuthal number of 1608 was 600.988 nm. For a microsphere in water, the resonant wavelength for the fundamental TE mode with an azimuthal number of 1608 was 601.294 nm. The difference between the resonant wavelengths was 0.25 nm.

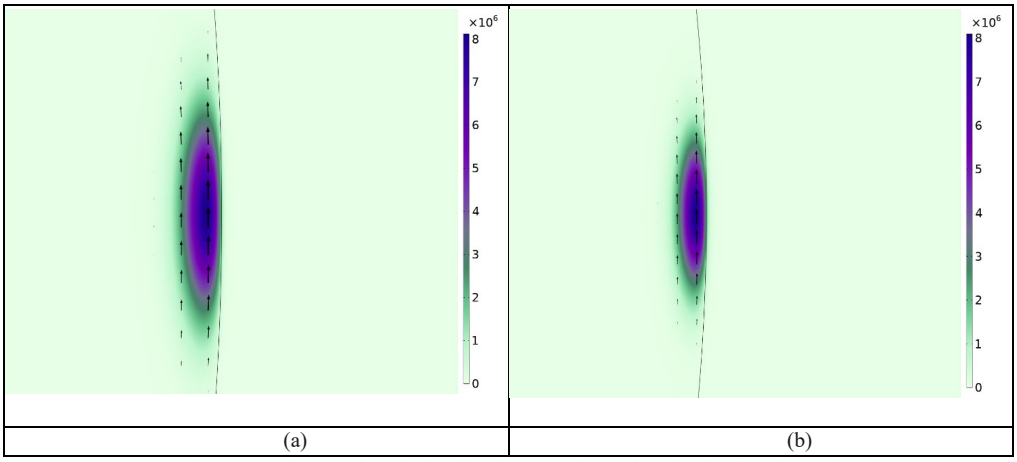

Fig. 34. Fundamental mode localization: (a) microsphere in air; (b) microsphere in water.

As a result of this study, a new material was obtained, which is suitable for use in label-free sensors with active WGM resonators. This material is very simple to obtain and cost-effective. The experiment showed that glass samples subjected to low-temperature ion exchange (LTIE) showed distinct absorption characteristics, particularly the absence of characteristic absorption peaks, which was attributed to the formation of Ag2...5 molecular clusters of silver. Luminescence measurements demonstrated a broad emission band in the visible spectrum, particularly in the 500–900 nm range, confirming the formation of silver microcrystals during the LTIE process. According to the simulation results, the difference in resonant wavelengths between media with different refractive indices was 0.26 nm. This allows the material to be used for microsphere sensors without requiring a direct physical connection. The results obtained demonstrate the potential of soda-lime silicate glass with molecular silver clusters as a material for whispering gallery mode (WGM) sensors.

CONCLUSIONS

This PhD Thesis presents theoretical predictions and practical validations of previously unexplored non-scattering regimes, specifically focusing on hybrid anapoles. These regimes require the simultaneous interference of electric and magnetic multipoles. The obtained results pave the way for the development of substrate-independent metasurfaces with dual functionality, as well as ultrafast modulation approaches. Furthermore, the study of spin-to-orbital angular momentum conversion has opened up new and exciting possibilities for directional fluid navigation on-chip and nanoscale fluid manipulation. Driven fluid flows and size separation within microfluidic systems are enabled by leveraging the optical properties of dielectric nanoantennas along with the dynamics induced by incident light. Additionally, the study of pulse propagation in resonant multilayered media with disorder distributions has revealed transitions and regimes that provide flexible control over the optical response of the medium.

These results have potential applications where controlling the reflection-to-transmission ratio and the propagation of ultrafast pulses in nanomaterials is crucial. Moreover, a novel method for contactless temperature and diffusion measurements is demonstrated by utilizing the Purcell effect in phosphorescent molecules near nanoantennae. This technique holds potential applications in microfluidics and lab-on-a-chip systems. Subwavelength nonspherical resonators are being used to explore superscattering regimes, highlighting increased multipolar resonances with applications ranging from biosensing to energy harvesting, on-chip circuitry, and optical manipulation. An understanding of transverse optical binding around hyperbolic metamaterials provides valuable insights into enhanced optomechanical manipulation techniques driven by high-k volumetric modes. Multiple reflections from boundaries are facilitated by thin metamaterial slabs, leading to highly localized hotspots with significant intensity gradients.

In summary, the combined results of this research contribute to the development of nanophotonics by revealing novel optical phenomena, simplifying the design of creative systems and devices, and providing access to a wide variety of applications in diverse fields. These findings provide a solid foundation for future research and development in ultrafast subwavelength optics and related fields as the discipline progresses.

BIBLIOGRAPHY

1. S. M. Kamali, E. Arbabi, A. Arbabi, and A. Faraon, "A review of dielectric optical metasurfaces for wavefront control", Nanophotonics, vol. 7, no. 6, 2018, pp. 1041–1068, DOI:https://doi.org/10.1515/nanoph-2017-0129

2. L. Khriachtchev, (2016). Silicon Nanophotonics: Basic Principles, Present Status, and Perspectives, Second Edition, Jenny Stanford Publishing, DOI: https://doi.org/10.1201/9781315364797

3. S. Jahani, Z. Jacob, "All-dielectric metamaterials," Nature Nanotech 11, 23–36 (2016), DOI:https://doi.org/10.1038/nnano.2015.304

4. P. Rufangura, T. Folland, A. Agrawal, J. Caldwell, F. Lacopi, "Towards low-loss on-chip nanophotonics with coupled graphene and silicon carbide: a review," Journal of Physics: Materials 3, 2020, DOI:10.1088/2515 7639/ab9d10

5. R. S. Savelev, D. S. Filonov, M. I. Petrov, A. E. Krasnok, P. A. Belov, Y. S. Kivshar, "Resonant transmission of light in chains of high-index dielectric particles," Physical Review B, " 2015, 92(15), pp. 1–5, 2015, DOI:https://doi.org/10.1103/PhysRevB.92.155415

6. R. Savelev, D. Filonov, P. Kapitanova, A. Krasnok, A. Miroshnichenko, P. Belov, Y. S. Kivshar, "Bending of electromagnetic waves in all-dielectric particle array waveguides," Applied Physics Letters. 105., (2014), DOI:https://doi.org/10.1063/1.4901264

7. O. Limon, L. Businaro, A. Gerardino, O. Bitton, A. Frydman, Z. Zalevsky, "Fabrication of electro optical nano modulator on silicon chip," Microelectronic Engineering 86, 1099–1102, (2009), DOI:https://doi.org/10.1016/j.mee.2009.01.007

8. A.E. Krasnok, A. E. Miroshnichenko, P. A. Belov, Y. S. Kivshar, "All-dielectric optical nanoantennas," Opt. Express 20, 20599–20604 (2012)

9. J. Henry, J. Livingstone, "Thin-Film Amorphous Silicon Position-Sensitive Detectors," Advanced Materials 13, (2001), 1022–1026, DOI: https://doi.org/10.1002/1521-4095(200107)13:12/133.0.CO;2-I

10. A.M., Miroshnichenko, A. E., Shadrivov, I. V. Shadrivov, Y. S. Kivshar, "All-Dielectric Multilayer Cylindrical Structures for Invisibility Cloaking," Sci. Rep. 5, (2015), DOI:https://doi.org/10.1038/srep09574

11. W. T. Chen, A. Y. Zhu, F. Capasso, "Flat optics with dispersion-engineered metasurfaces," Nat Rev Mater 5, 604–620, (2020), DOI:https://doi.org/10.1038/s41578-020-0203-3

12. D. Lin, P. Fan, E. Hasman, M. L. Brongersma, "Dielectric gradient metasurface optical elements," Science, Jul. 18, 2014, 345(6194): 298–302, DOI:10.1126/science.1253213

13. E. Nazemosadat, M. Mazur, S. Kruk, I. Kravchenko, J. Carpenter, J. Schröder, P. Andrekson, M. Karlsson, Y. S. Kivshar, "Dielectric Broadband Metasurfaces for Fiber Mode-Multiplexed Communications," Advanced Optical Materials. 7, (2019), DOI: https://doi.org/10.1002/adom. 201801679

14. J. Yan, J., Liu, X., Ma, C., Huang, Y., Yang, G., “All-dielectric materials and related nanophotonic applications”, (2020) Materials Science and Engineering R: Reports, 141, art. no. 100563. doi: 10.1016/j.mser.2020.100563

15. Kamali, S.M., Arbabi, E., Arbabi, A., Faraon, A., “A review of dielectric optical metasurfaces for wavefront control”, (2018) Nanophotonics, 7 (6), pp. 1041-1068.doi: 10.1515/nanoph-2017-0129

16. M. L. Brongersma, “The road to atomically thin metasurface optics”, Nanophotonics 10, 643–654 (2020).

17. D. G. Baranov, D. A. Zuev, S. I. Lepeshov, O. V. Kotov, A. E. Krasnok, A. B. Evlyukhin, and B. N. Chichkov, “All-dielectric nanophotonics: the quest for better materials and fabrication techniques” Optica 4, 814-825 (2017).

18. S. Liu, M. B. Sinclair, S. Saravi, G. A. Keeler, Y. Yang, J. Reno, G. M. Peake, F. Setzpfandt, I. Staude, T. Pertsch, and I. Brener, “Resonantly enhanced second-harmonic generation using III-V semiconductor all-dielectric metasurfaces”, Nano Lett. 16, 5426–5432 (2016).

19. R. S. Savelev, D. S. Filonov, P. V. Kapitanova, A. E. Krasnok, A. E. Miroshnichenko, P. A. Belov, and Y. S. Kivshar, “Bending of electromagnetic waves in all-dielectric particle array waveguides”, Appl. Phys. Lett. 105, (2014).

20. R. M. Bakker, Y. F. Yu, R. Paniagua-Domínguez, B. Luk’yanchuk, and A. I. Kuznetsov, “Resonant light guiding along a chain of silicon nanoparticles”, Nano Lett. 17, 3458–3464 (2017).

21. Y. H. Fu, A. I. Kuznetsov, A. E. Miroshnichenko, Y. F. Yu, and B. Luk’yanchuk, “Directional visible light scattering by silicon nanoparticles”, Nat. Commun. 4, 1527 (2013).

22. K. Chen, Y. Feng, F. Monticone, J. Zhao, B. Zhu, T. Jiang, L. Zhang, Y. Kim, X. Ding, S. Zhang, A. Alù, and C. W. Qiu, “A Reconfigurable Active Huygens' Metalens”, Adv. Mater. 29, 1–7 (2017).

23. K. Koshelev, S. Kruk, E. Melik-Gaykazyan, J. H. Choi, A. Bogdanov, H. G. Park, and Y. Kivshar, “Subwavelength dielectric resonators for nonlinear nanophotonics”, Science (80-.). 367, 288–292 (2020).

24. A.S. Shalin, “Microscopic theory of optical properties of composite media with chaotically distributed nanoparticles”, Quantum Electron. 40, 1004–1011 (2010).

25. P. M. Voroshilov, C. R. Simovski, P. A. Belov, and A. S. Shalin, “Light-trapping and antireflective coatings for amorphous Si-based thin film solar cells”, J. Appl. Phys. 117, (2015).

26. Y. Cui, D. van Dam, S. A. Mann, N. J. J. van Hoof, P. J. van Veldhoven, E. C. Garnett, E. P. A. M. Bakkers, and J. E. M. Haverkort, “Boosting solar cell photovoltage via nanophotonic engineering”, Nano Lett. 16, 6467–6471 (2016).

27. P. D. Terekhov, K. V. Baryshnikova, Y. Greenberg, Y. H. Fu, A. B. Evlyukhin, A. S. Shalin, and A. Karabchevsky, “Enhanced absorption in all-dielectric metasurfaces due to magnetic dipole excitation”, Sci. Rep. 9, 3438 (2019).

28. J. Algorri, D. Zografopoulos, A. Ferraro, B. García-Cámara, R. Vergaz, R. Beccherelli, and J. Sánchez-Pena, “Anapole modes in hollow nanocuboid dielectric metasurfaces for refractometric sensing”, Nanomaterials 9, 30 (2018).

29. S. Jahani, and Z. Jacob, “All-dielectric metamaterials”, Nat. Nanotechnol. 11, 23–36 (2016).

30. H. K. Shamkhi, K. V. Baryshnikova, A. Sayanskiy, P. Kapitanova, P. D. Terekhov, P.

Belov, A. Karabchevsky, A. B. Evlyukhin, Y. Kivshar, and A. S. Shalin, “Transverse Scattering and Generalized Kerker Effects in All-Dielectric Mie-Resonant Metaoptics”, Phys. Rev. Lett. 122, 193905 (2019).

31. D. Wang, Q. Fan, J. Wang, Z. Zhang, Y. Liang, and T. Xu, “All-dielectric metasurface beam deflector at the visible frequencies”, Guangdian Gongcheng/Opto-Electronic Eng. 44, 103–107 (2017).

32. P. Grahn, A. Shevchenko, and M. Kaivola, “Electromagnetic multipole theory for optical nanomaterials”, New J. Phys. 14, (2012).

33. R. Alaee, C. Rockstuhl, and I. Fernandez-Corbaton, “An electromagnetic multipole expansion beyond the long-wavelength approximation”, Opt. Commun. 407, 17–21 (2018).

34. A.B. Evlyukhin, T. Fischer, C. Reinhardt, and B. N. Chichkov, “Optical theorem and multipole scattering of light by arbitrarily shaped nanoparticles”, Phys. Rev. B 94, 1–7 (2016).

35. R. E. Raab, and O. L. Lange, Multipole Theory in Electromagnetism (Oxford Science Publications, New York, n.d.).

36. J. D. Jackson, Classical Electrodynamics, 3rd ed. (New York, {NY}, 1999).

37. N. Papasimakis, V. A. Fedotov, V. Savinov, T. A. Raybould, and N. I. Zheludev, “Electromagnetic toroidal excitations in matter and free space”, Nat. Mater. 15, 263–271 (2016).

38. V. M. Dubovik, and V. V. Tugushev, “Toroid Moments in Electrodynamics and Solid-State Physics”, Phys. Rep. 187, 145–202 (1990).

39. T. Góngora, and E. Ley-Koo, “Complete electromagnetic multipole expansion including toroidal moments”, Rev. Mex. Fis. E 52, 188–197 (2006).

40. V. A. Fedotov, A. V. Rogacheva, V. Savinov, D. P. Tsai, and N. I. Zheludev, “Resonant Transparency and Non-Trivial Non-Radiating Excitations in Toroidal Metamaterials”, Sci. Rep. 3, 1–5 (2013).

41. W. Liu, B. Lei, J. Shi, H. Hu, and A. E. Miroshnichenko, “Elusive Pure Anapole

42. Excitation in Homogenous Spherical Nanoparticles with Radial Anisotropy”, J. Nanomater. 2015, 382 (2015).

43. W. Liu, J. Zhang, B. Lei, H. Hu, and A. E. Miroshnichenko, “Invisible nanowires with interfering electric and toroidal dipoles”, Opt. Lett. 40, 2293 (2015).

44. J. Tian, H. Luo, Y. Yang, F. Ding, Y. Qu, D. Zhao, M. Qiu, and S. I. Bozhevolnyi, “Active control of anapole states by structuring the phase-change alloy $Ge_2Sb_2Te_5$”, Nat. Commun. 10, 1–9 (2019).

45. K. Ospanova, I. V. Stenishchev, and A. A. Basharin, “Anapole mode sustaining silicon metamaterials in visible spectral range”, Laser Photon. Rev. 12, 1800005 (2018).

46. N. A. Nemkov, A. A. Basharin, and V. A. Fedotov, “Electromagnetic sources beyond common multipoles”, Phys. Rev. A 98, 1–9 (2018).

47. E. A. Gurvitz, K. S. Ladutenko, P. A. Dergachev, A. B. Evlyukhin, A. E. Miroshnichenko, and A. S. Shalin, “The high-order toroidal moments and anapole states in all-dielectric photonics”, Laser Photon. Rev. 13, 1800266 (2019).

48. S. Gladyshev, K. Frizyuk, and A. Bogdanov, “Symmetry analysis and multipole classification of eigenmodes in electromagnetic resonators for engineering their optical

properties", Phys. Rev. B 102, 075103 (2020).

49. E. Takou, A. C. Tasolamprou, O. Tsilipakos, and E. N. Economou, "Dynamic anapole in metasurfaces made of sculptured cylinders", Phys. Rev. B 100, 085431 (2019).

50. G. Grinblat, Y. Li, M. P. Nielsen, R. F. Oulton, and S. A. Maier, "Enhanced Third Harmonic Generation in Single Germanium Nanodisks Excited at the Anapole Mode", Nano Lett. 16, 4635–4640 (2016).

51. T. Shibanuma, G. Grinblat, P. Albella, and S. A. Maier, "Efficient Third Harmonic Generation from Metal–Dielectric Hybrid Nanoantennas", Nano Lett. 17, 2647–2651 (2017).

52. S. V. Makarov, M. I. Petrov, U. Zywietz, V. Milichko, D. Zuev, N. Lopanitsyna, A. Kuksin, I. Mukhin, G. Zograf, E. Ubyivovk, D. A. Smirnova, S. Starikov, B. N. Chichkov, and Y. S. Kivshar, "Efficient Second-Harmonic Generation in Nanocrystalline Silicon Nanoparticle", Nano Lett. 17, 3047–3053 (2017).

53. A.Kaldun, A. Blättermann, V. Stooß, S. Donsa, H. Wei, R. Pazourek, S. Nagele, C. Ott, C. D. Lin, J. Burgdörfer, and T. Pfeifer, "Observing the ultrafast buildup of a Fano resonance in the time domain", Science 354, 738–741 (2016).

54. S. Lepeshov, and A. Krasnok, "Virtual Optical Pulling Force", Optica 7, 1024-1030 (2020).

55. S. A. Maier, M. P. Nielsen, G. Grinblat, Y. Li, and R. F. Oulton, "Efficient third harmonic generation and nonlinear subwavelength imaging at a higher-order anapole mode in a single germanium nanodisk", ACS Nano 11, 953–960 (2016).

56. Z.-J. Yang, Y.-H. Deng, Y. Yu, and J. He, "Magnetic toroidal dipole response in individual all-dielectric nanodisk clusters", Nanoscale 12, 10639–10646 (2020).

57. B. Luk'yanchuk, R. Paniagua-Domínguez, A. I. Kuznetsov, A. E. Miroshnichenko, and Y. S. Kivshar, "Hybrid anapole modes of high-index dielectric nanoparticles", Phys. Rev. A 95, 1–8 (2017).

58. K. Ospanova, A. Basharin, A. E. Miroshnichenko, and B. Luk'yanchuk, "Generalized hybrid anapole modes in all-dielectric ellipsoid particles", Opt. Mater. Express 11, 23-34 (2021).

59. E. A. Gurvitz, K. S. Ladutenko, P. A. Dergachev, A. B. Evlyukhin, A. E. Miroshnichenko, and A. S. Shalin, "The high-order toroidal moments and anapole states in all-dielectric photonics", Laser Photonics Rev. 13, 1800266 (2019).

60. W. Yan, R. Faggiani, and P. Lalanne, "Rigorous modal analysis of plasmonic nanoresonators", Phys. Rev. B 97, 205422 (2018).

61. P. Lalanne, W. Yan, K. Vynck, C. Sauvan, and J. P. Hugonin, "Light interaction with photonic and plasmonic resonances", Laser Photonics Rev. 12, 1–38 (2018).

62. M. I. Tribelsky, and A. E. Miroshnichenko, Phys. Rev. A 100, 1–5 (2019).

63. O. Ávalos-Ovando, L. V. Besteiro, Z. Wang, and A. O. Govorov, "Temporal plasmonics: Fano and Rabi regimes in the time domain in metal nanostructures", ArXiv 9, 3587–3595 (2020).

64. M. I. Tribelsky, and A. E. Miroshnichenko, "Giant in-particle field concentration and Fano resonances at light scattering by high-refractive-index particles", Phys. Rev. A 93, 053837 (2016).

65. L. Wei, Z. Xi, N. Bhattacharya, and H. P. Urbach, “Excitation of the radiationless anapole mode”, Optica 3, 799-802 (2016).

66. J. A. Parker, H. Sugimoto, B. Coe, D. Eggena, M. Fujii, N. F. Scherer, S. K. Gray, and U. Manna, “Excitation of nonradiating anapoles in dielectric nanospheres”, Phys. Rev. Lett. (2020).

67. V. A. Zenin, S. M. Novikov, Y. Yang, B. N. Chichkov, S. I. Bozhevolnyi, A. B. Evlyukhin, R. Malureanu, and A. V Lavrinenko, “Direct amplitude-phase near-field observation of higher-order anapole states”, Nano Lett. 17, 7152–7159 (2017).

68. M. I. Tribelsky, and A. E. Miroshnichenko, “Giant in-particle field concentration and Fano resonances at light scattering by high-refractive-index particles”, Phys. Rev. A 93, 053837 (2016).

69. Garcés-Chávez, V., Volke-Sepulveda, K., Chávez-Cerda, S., Sibbett, W. & Dholakia, K. Transfer of orbital angular momentum to an optically trapped low-index particle. Phys. Rev. A - At. Mol. Opt. Phys. 66, 8 (2002).

70. Sokolovskii, G. S. et al. Bessel beams from semiconductor light sources. Prog. Quantum Electron. 38, 157–188 (2014).

71. Shamkhi, H. K. et al. Transverse scattering and generalized kerker effects in all-dielectric mie-resonant metaoptics. Phys. Rev. Lett. 122, 1–22 (2019).

72. Donner, J. S., Baffou, G., McCloskey, D. & Quidant, R. Plasmon-assisted optofluidics. ACS Nano 5, 5457–5462 (2011).

73. Huang, C., Chen, X., Oladipo, A. O., Panoiu, N. C. & Ye, F. Generation of Subwavelength Plasmonic Nanovortices via Helically Corrugated Metallic Nanowires. Sci. Rep. 5, 1–10 (2015).

74. David, A., Gjonaj, B. & Bartal, G. Two-dimensional optical nanovortices at visible light. Phys. Rev. B 93, 1–5 (2016).

75. Young, A. B. et al. Polarization Engineering in Photonic Crystal Waveguides for Spin-Photon Entanglers. Phys. Rev. Lett. 115, 1–5 (2015).

76. David, A., Gjonaj, B., Blau, Y., Dolev, S. & Bartal, G. Nanoscale shaping and focusing of visible light in planar metal–oxide–silicon waveguides. Optica 2, 1045 (2015).

77. Willig, K. I. et al. Nanoscale resolution in GFP-based microscopy. Nat. Methods 3, 721–723 (2006).

78. Chithrani, B. D., Ghazani, A. A. & Chan, W. C. W. Determining the size and shape dependence of gold nanoparticle uptake into mammalian cells. Nano Lett. 6, 662–668 (2006).

79. Chithrani, B. D. & Chan, W. C. W. Elucidating the mechanism of cellular uptake and removal of protein-co

80. Pan, Y. et al. Size-dependent cytotoxicity of gold nanoparticles. Small 3, 1941–1949 (2007).

81. Kern, A. M. & Martin, O. J. F. Excitation and reemission of molecules near realistic plasmonic nanostructures. Nano Lett. 11, 482–487 (2011).

82. S. A. Gredeskul, Yu. S. Kivshar, A. A. Asatryan, K. Y. Bliokh, Yu. P. Bliokh, V. D. Freilikher, I. V. Shadrivov, Low Temp. Phys. 2012, 38, 570.

83. H. H. Scheinfux, Y. Lumer, G. Ankonina, A. Z. Genack, G. Bartal, M. Segev, Science

2017, 356, 953.

84. C. Liu, W. Gao, B. Yang, S. Zhang, Phys. Rev. Lett. 2017, 119, 183901.

85. H. H. Scheinfux, I. Kaminer, A. Z. Genack, M. Segev, Nat. Commun. 2016, 7, 12927.

86. M. Jang, Y. Horie, A. Shibukawa, J. Brake, Y. Liu, S. M. Kamali, A. Arbabi, H. Ruan, A. Faraon, C. Yang, Nat. Photon. 2018, 12, 84.

87. L. Allen, J. H. Eberly, Optical Resonance and Two-Level Atoms, Wiley, New York 1975.

88. S. L. McCall, E. L. Hahn, Phys. Rev. 1969, 183, 457.

I. A. Poluektov, Yu. M. Popov, V. S. Roitberg, Sov. Phys. Usp. 1975, 17, 673.

89. R. M. Arkhipov, M. V. Arkhipov, I. Babushkin, A. Demircan, U. Morgner, N. N. Rosanov, Opt. Lett. 2016, 41, 4983.

90. R. M. Arkhipov, A. V. Pakhomov, M. V. Arkhipov, I. Babushkin, A. Demircan, U. Morgner, N. N. Rosanov, Sci. Rep. 2017, 7, 12467.

91. A.A. Afanas'ev, V. M. Volkov, V. V. Dritz, B. A. Samson, J. Mod. Opt. 1990, 37, 165.

92. M. J. Shaw, B. W. Shore, J. Opt. Soc. Am. B 1991, 8, 1127.

93. D. V. Novitsky, Phys. Rev. A 2011, 84, 013817.

94. D. V. Guzatov, S. V. Vaschenko, V. V. Stankevich, A. Y. Lunevich, Y. F. Glukhov, and S. V. Gaponenko, J. Phys. Chem. C 116, 10723 (2012).

95. A.N. Poddubny, P. Ginzburg, P. A. Belov, A. V. Zayats, and Y. S. Kivshar, Phys. Rev. A At. Mol. Opt. Phys. 86, 033826 (2012).

96. Ivinskaya, A.; Kostina, N.; Proskurin, A.; Petrov, M. I.; Bogdanov, A. A.; Sukhov, S.; Krasavin, A. V.; Karabchevsky, A.; Shalin, A. S.; Ginzburg, P. Optomechanical Manipulation with Hyperbolic Metasurfaces. ACS Photonics 2018, 5 (11), 4371−4377.

97. Johnson, P. B.; Christy, R. W. Optical Constants of the Noble Metals. Phys. Rev. B 1972, 6 (12), 4370−4379.

98. Rodríguez-de Marcos, L. V.; Larruquert, J. I.; Mendez, J. A.;́Aznarez, J. A. Self-Consistent Optical Constants of SiO_2 and ́Ta_2O_5 Films. Opt. Mater. Express 2016, 6 (11), 3622.

99. Rybin, M. V. et al. High- Q supercavity modes in subwavelength dielectric resonators. Phys. Rev. Lett. 119, 1–5 (2017).

100. Friedrich, H. Interfering resonances and BIC. Phys. Rev. A 32, 3231–3242 (1985).

101. Gladyshev, S., Frizyuk, K. & Bogdanov, A. Symmetry analysis and multipole classification of eigenmodes in electromagnetic resonators for engineering their optical properties. Phys. Rev. B 102,075103 (2020).

102. Kostina, N. et al. Optical binding via surface plasmon polariton interference. Phys. Rev. B 99, 125416 (2017).

103. Barhom, H. et al. Biological Kerker effect boosts light collection efficiency in plants. Nano Lett 19, 7062–7071 (2019).

104. Terekhov, P. D. et al. Broadband forward scattering from dielectric cubic nanoantenna in lossless media. Opt. Express 27, 10924 (2019).

105. Terekhov, P. D. et al. Enhanced absorption in all-dielectric metasurfaces due to magnetic dipole excitation. Sci. Rep. 9, 3438 (2019).

106. Kozlov, V., Filonov, D., Shalin, A. S., Steinberg, B. Z., & Ginzburg, P. Asymmetric backscattering from the hybrid magneto-electric metaparticle. Appl. Phys. Lett. 109, 203503 (2016).

107. Guo, R. et al. High–bit rate ultra-compact light routing with mode-selective on-chip nanoantennas. Sci. Adv. 3, e1700007 (2017).

108. Wang, S. B. & Chan, C. T. Lateral optical force on chiral particles near a surface. Nat. Commun. 5, 1–8 (2014).

109. Kislov, D. A. et al. Multipole engineering of attractive−repulsive and bending optical forces. Adv. Photonics Res. 2, 2100082 (2021).

110. E. D. Palik, Handbook of Optical Constants of Solids: Handbook of Thermo-Optic Coefficients of Optical Materials with Applications, Elsevier, New York 1997.

111. Sheng, J.; Li, J.; Yu, J. The development of silver nanoclusters in ion-exchanged soda-lime silicate glasses. Int. J. Hydrog. Energy 2007, 32, 2598–2601.

112. Simo, A.; Polte, J.; Pfander, N.; Vainio, U.; Emmerling, F.; Rademann, K. Formation Mechanism of Silver Nanoparticles Stabilized in Glassy Matrices. J. Am. Chem. Soc. 2012, 134, 18824–18833.

Dmitrii Redka was born in 1989 in Germany. He received a Master's degree in Quantum and Optical Electronics (2010) from Saint Petersburg State Electrotechnical University (Russia). He is currently a researcher at the Institute of Photonics, Electronics and Telecommunications of RTU Faculty of Computer Science, Information Technology and Energy.